DOE/NASA/0351-1
NASA CR-174994

Experimental Assessment of Advanced Stirling Component Concepts

B. Ziph
Stirling Thermal Motors, Inc.

October 1985

Prepared for
NATIONAL AERONAUTICS AND SPACE ADMINISTRATION
Lewis Research Center
Under Contract DEN 3-351

for
U.S. DEPARTMENT OF ENERGY
Conservation and Renewable Energy
Office of Vehicle and Engine R&D

DISCLAIMER

Printed in the United States of America

Available from
National Technical Information Service
U S Department of Commerce
5285 Port Royal Road
Springfield, VA 22161

NTIS price codes[1]
Printed copy A06
Microfiche copy A01

[1]Codes are used for pricing all publications The code is determined by the number of pages in the publication Information pertaining to the pricing codes can be found in the current issues of the following publications, which are generally available in most libraries *Energy Research Abstracts (ERA), Government Reports Announcements* and Index (*GRA* and I), *Scientific and Technical Abstract Reports (STAR),* and publication, NTIS-PR-360 available from NTIS at the above address

DOE/NASA/0351-1
NASA CR-174994

Experimental Assessment of Advanced Stirling Component Concepts

B. Ziph
Stirling Thermal Motors, Inc.
Ann Arbor, Michigan 48104

October 1985

Prepared for
National Aeronautics and Space Administration
Lewis Research Center
Cleveland, Ohio 44135
Under Contract DEN 3-351

for
U.S. DEPARTMENT OF ENERGY
Conservation and Renewable Energy
Office of Vehicle and Engine R&D
Washington, D.C. 20545
Under Interagency Agreement DE-AI01-77CS51040

TABLE OF CONTENTS

SECTION 1 - BACKGROUND AND INTRODUCTION

There are several Stirling engine technology concepts which Stirling Thermal Motors, Inc. (STM) of Ann Arbor, Michigan, has advanced. These technologies, if they achieve their potential, should contribute significantly to the Department of Energy (DOE) funded Automotive Stirling engine (ASE) program.

Some of the most promising technologies which STM has proposed for investigation include:

1. Pressurized crankcase with rotating shaft seal
2. Advanced piston rings with improved performance
3. Piston rod scraper seal
4. Heat pipes to transport energy into the engine

The current ASE relies on reciprocating piston rod seals to contain the working gas. The life potential of these seals has not been demonstrated to meet the 3500 hour goal of the ASE program. STM has proposed an alternate approach to dynamic seals currently not being pursued in the ASE program, where the crankcase is pressurized to the mean cycle pressure and the working gas is contained by a high pressure rotating seal on the engine output shaft. These rotating seals are commercially available and have a manufacturer's claimed life potential of more than 10,000 hours. For this concept, a reciprocating piston rod seal consisting of a cap seal and oil scraper is still needed. But, it is needed only to isolate the varying cycle pressures from the constant crankcase pressure and to prevent oil from entering the thermodynamic cycles.

The use of a pressurized crankcase, however, precludes controlling engine power by varying the engine pressure as currently is done in the ASE - mainly because of the complications of handling the oil entrained as a mist in the working gas in the crankcase. Therefore, an alternate means of power control is

used where the pressure remains constant and the piston stroke is varied. The variable stroke can be accomplished by using a variable angle swashplate drive. STM has developed a design for the system needed to control the variable stroke drive which is quite simple and has a potential cost and reliability advantage compared to the system required to vary engine pressure. The variable swashplate drive also has the additional potential advantages of being self-starting and of having better part load engine efficiency than a fixed stroke engine.

The inherent characteristics of the swashplate drive are such that the main drive shaft is subjected to large bending moments. As a result the unsupported end of the shaft at the rotating seal location tends to deflect more than the amount the seal can tolerate without affecting life and leakage rate. Therefore, a means is needed to eliminate shaft run out at the rotating seal. STM has proposed such a design using a split shaft.

Another area of interest in the ASE program is piston rings. Piston ring friction life and sealing efficinecy are important factors in meeting the ASE fuel economy goals. STM has proposed the use of a solid single piston ring (the current ASE uses two rings) with a means for controlling the contact force against the cylinder wall which potentially would produce an improvement in engine fuel economy. STM has also proposed a number of alternative piston-ring designs and concepts all aimed at bringing about improvement in engine efficiency through reduced friction and leakage in the piston rings.

The use of heat pipes offers a number of potential advantages for the ASE as well as for other Stirling engine applications:

- It provides considerable flexiblity to allow for packaging requirements and ease of manufacturing.
- It allows major simplification of heat exchanger design. An engine heater, designed to take advantage of the high film heat transfer

coefficient of condensing metal vapor can be considerably less expensive and more suitable for mass production than conventional heaters such as those used for the ASE.

- It brings about considerable improvement to the engine performance by permitting the heater design to be ideally suited to the thermodynamic requirements.
- The uniform temperature throughtout the confines of the heat-pipe enclosure eliminates hot spots on the heater and thus enhances both the efficiency and the reliability of the engine.

Conventional heat pipe designs require a lengthy procedure for charging. The procedure requires evacuation to a hard vacuum and bake out at elevated temperature to remove gases entrapped within the surface of the metal container. This process generally is not suiteable for volume production as required for an ASE. The use of a getter within the heat pipe, as proposed by STM, may eliminate or reduce the bake out requirement and eliminate the need for special production equipment. Also, the use of a mechanical coupling to join heat pipe sections also proposed by STM would allow the sections to be made as simple subassemblies, thus greatly reducing the potential part rejection rate.

In an unsolicited proposal, Stirling Thermal Motors, Inc. has proposed to do analysis, design, fabrication and testing of components meeting the needs of the advanced concepts discussed above. Under the resulting Contract No. DEN3-351 the following areas were investigated:

1) Piston Rings

Two advanced piston ring concepts were experimentally assessed and compared to conventional piston rings (the performance of which was

measured on the same rig to establish a base-line).

- Single, solid piston ring with a bi-metal spring proved impractical in view of its very high sensitivity to the operating temperature.
- A bonded piston ring set, in preliminary testing, proved a very promising concept exhibiting relatively low losses.

2) Reciprocating Rod Seal

A babbit scraper mounted in a compliant housing was subjected to long term endurance tests at atmospheric pressure. Test conditions provided lateral motion of the rod which is of about twice the amplitude expected in an engine. The seal operated for 6750 essentially trouble-free hours.

Use of the scraper seal as a gas pressure containment seal was also investigated experimentally. Whereas it did not perform adequately as a containment seal the tests pointed out some modifications which may adapt it successfully to such application.

3) Heat Pipes

Twelve heat pipes were built and six were subjected to long-term endurance testing, clearly indicating the adequacy of the simple, inexpensive fabrication and filling procedures used. In addition the tests proved the effectiveness of getters in rendering the heat pipe rather tolerant to air leakage and making it possible to avoid furnace degassing during fabrication.

Commercially available mechanical couplings were demonstrated to be applicable to the heat pipes. They proved tolerant of thermal

cycling and able to readily provide capillary connection.

4) Split Shaft Component Design

A split shaft with a separate end seal assembly was designed in detail based upon a reference design (STM4-120 variable swashplate Stirling engine) previously generated by STM. The design fully meets all the criteria, solves the shaft run out problem at the seal area and ensures component life greater than 10,000 hours at full load.

The advanced concepts tested, the tests themselves, and their results are described in detail in this report. The following Sections 2 through 5 describe the piston rings tests, rod seal tests, heat pipe tests, and split shaft design, respectively.

SECTION 2 -PISTON RINGS

2.1 - Introduction and Summary

Whereas the traditional arrangement of two unidirectional ("pumping") piston rings shown in Figure 2.1 works well and reliably it does give rise to relatively high friction and leakage losses. These losses have been generally accepted as the unavoidable penalty which one has to pay in order to have high reliability, long life and the virtual elimination of net mass transfer across the piston rings which characterise the unidirectional ring arrangement.

The program described below, challenging the inevitability of the friction and leakage losses, was aimed at the development of an alternative ring arrangement which will reduce these losses.

At the beginning of the program it appeared that the concept of a single, solid, pressure-balanced piston ring backed up by a bimetallic spring showed great promise of reducing both friction and leakage while effectively eliminating net mass transfer. This ring, described in Section 2.2 below was tested with rather disappointing results.

It turned out that the stiffness of the closed ring played a major role, and, in combination with the large difference between the coefficient of thermal expansion of the ring material (Rulon LD) and that of the steel cylinder, yielded totally unreproducible results. The performance was so sensitive to temperature and fabrication tolerances (of the OD) that after testing with various modifications it became evident that a solid ring cannot be used adventageously or, at least, that some basic new approach to such a ring is required.

Since such basic new approach remained elusive the effort was concentrated on modifications to the split unidirectional rings arrangement with the purpose

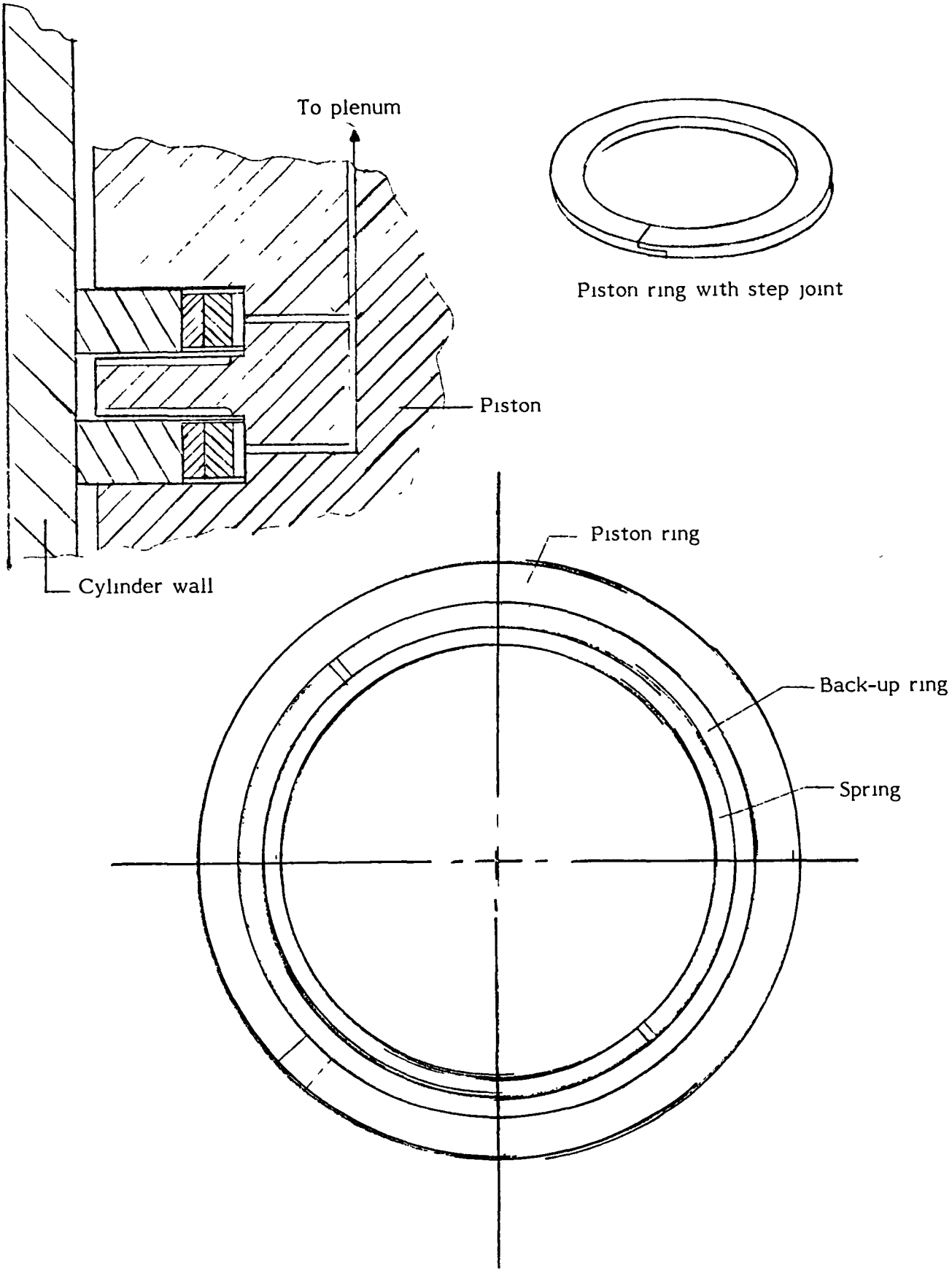

Figure 2.1

Traditional arrangement of two unidirectional "pumping"piston rings (schematic)

of reducing friction and leakage.

It was postulated that the split rings allow leakage predominantly through the step joint. An effort focused on the joint, if successful in reducing the leakage thereat, will make it possible to reduce the axial thickness of the ring without adversely effecting the leakage, and thus will reduce friction.

A test program was, consequently, defined aimed at proving the following:

1) Leakage losses are governed by the step-joint quality and are, by and large, independent of the axial thickness of the ring.
2) Fricton losses are proportional to the axial thickness of the rings.

In order to prove the above statements, friction and leakage data were measured for the following three sets of rings:

1) Ring Set # 1 was fabricated by Shamban to STM dimensional specifications using common fabrication procedures. No particular attention was paid to the flatness or smoothness of the step joint. These rings had an effective axial thickness of 1.5 mm.
2) Ring Set #2 was made in-house. The step-joint surfaces were carefully cut and polished. The axial thickness was 2.4 mm.
3) Ring Set #3 is the same as Ring Set #2 except that the axial thickness is 3.7 mm.

The results clearly demonstrated that the quality of the step joint surface had a major influence on the leakage, that the axial thickness of the rings had only a minor influence on the leakage and that, as expected, the friction is proportional to the axial thickness of the ring.

In accordance with the above conclusions, a fourth set of bonded rings, described in detail in Section 2.3 below, was made and tested. These rings

are axially thin (1.7mm) and their step joints are well sealed.

Preliminary results demonstrate that, as expected, the friction is low, in accordance with the small axial thickness, and the leakage is not higher than that of much thicker rings. These rings (hereinafter "bonded rings") show significant promise. In addition to their high performance potential they require only a single groove in the one-piece piston and can accomodate a large amount of wear with no adverse influence on their performance. It is strongly recommended that further development of the bonded rings be undertaken.

2.2 - Single, Solid, Pressure-Balanced Piston Ring

The single, solid, pressure-balanced piston ring is shown schematically in Figure 2.2. Its design addresses the following issues:

a) The ring being closed, and thus having no joint, it should reduce the leakage substantially since, as was stipulated and later proven, it is the joint that provided the most important leak path.

b) The axial face of the ring being uninterrupted, since the ring is closed, can be positively sealed with an O-ring, eliminating the mechanism that may cause net mass transfer across the ring. Since the ring will not permit net mass transfer only a single ring is necessary rather than a set of two.

c) The geometry of the ring ensures that, practically, no net force is exerted on it by the gas pressure as shown in Figure 2.3. The contact force at the cylinder wall may be provided by a back-up spring. That force could be rather small and hence the friction loss will be minimal. Furthermore, that low friction is independent of the axial thickness of the ring which may thus be rather large to reduce leakage even further.

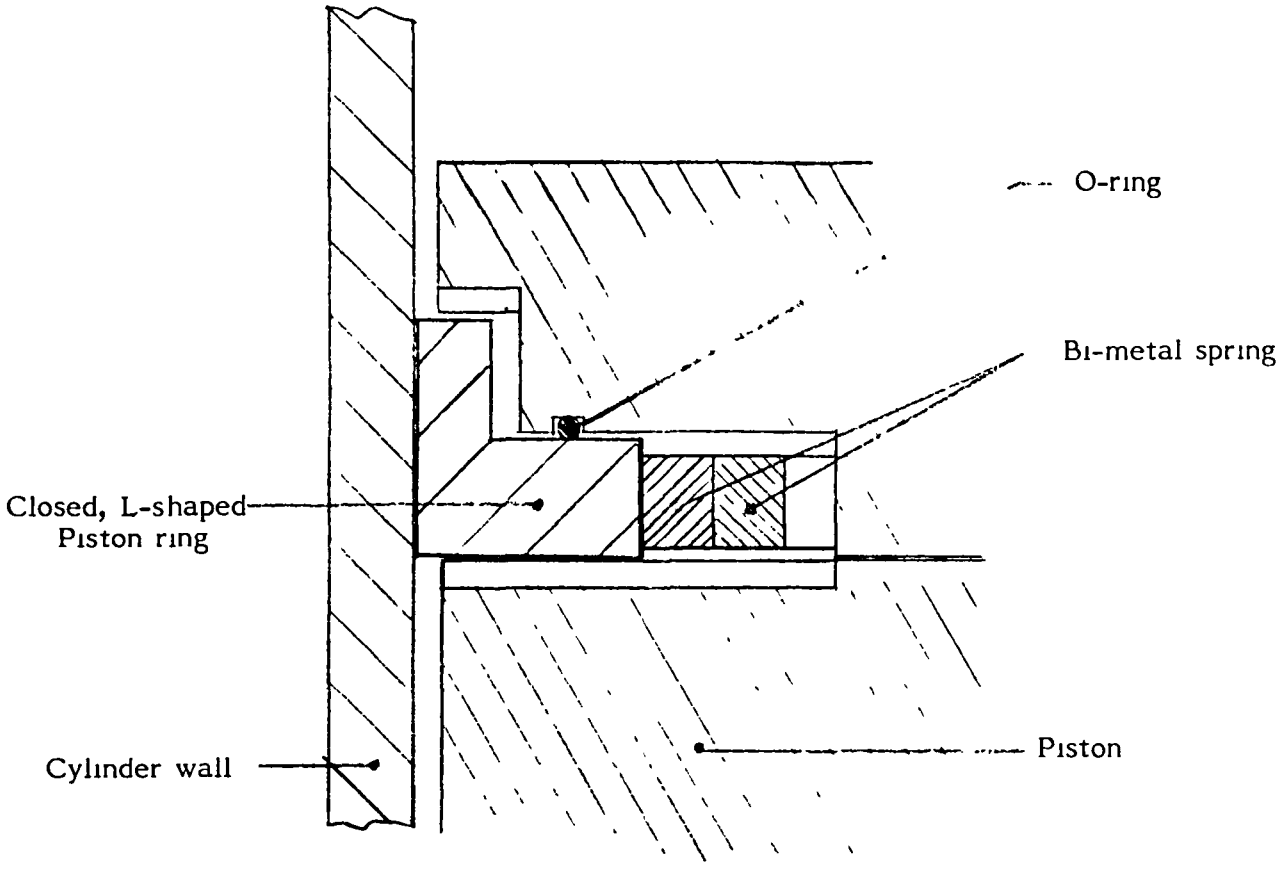

Figure 2.2

Single, solid, pressure balanced piston ring with bi-metallic back-up spring

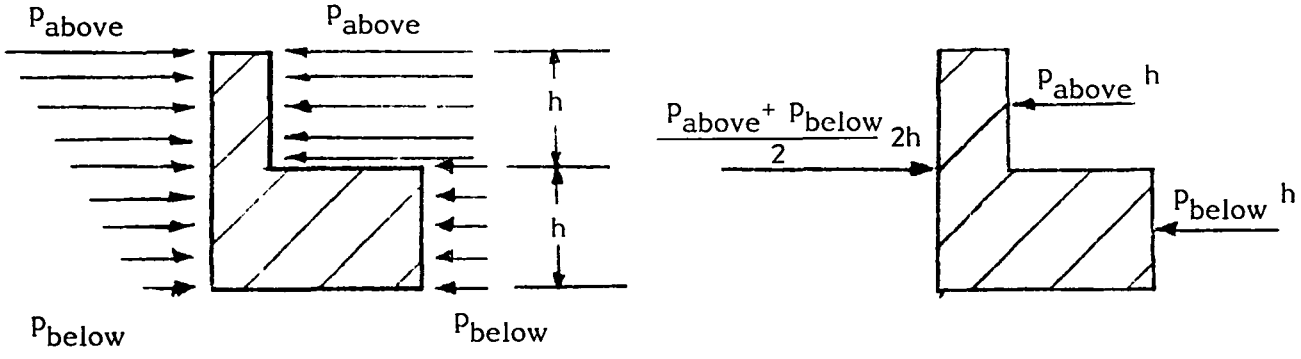

Figure 2.3

Balancing of pressure load on the balanced piston ring

Any closed piston ring is necessarily associated with a cold-start failure unless some action is taken to prevent such failure. The problem is caused by the coefficient of thermal expansion of the ring material which is much larger than that of the cylinder. As the operating temperature increases, the cylinder wall restrains the piston ring and prevents it from expanding. The ring develops compressive stress which after some time at the operating temperature will be relieved. Upon shut-down and cooling of the ring to ambient temperature the ring will shrink diametrically and lose contact with the wall. Sealing could not be established upon subsequent start-up attempt and the engine would not start.

To prevent this cold-start failure the piston ring is backed up by a bi-metallic spring as shown in Figure 2.2. Upon cold-start, at low temperature, the spring force will force the piston ring against the wall, ensuring successful start-up. As the operating temperature increases and the piston ring expands the free diameter of the bi-metal spring will contract resulting in a reduction of the contact force so that at operating temperature only a small force will remain. The friction under operating conditions will be minimal.

Testing of the single, solid, pressure-balanced piston rings with the bi-metal spring revealed that, in practice, the combination of the stiffness of the ring itself, the bi-metal spring constant and the tolerence of the dimension of the outer diameter of the piston ring created a situation where the behavior of the ring is extremely sensitive to the operating temperature.

In some cases as the operating temperature was rising from start-up compressive stress in the ring and the attandant rise in friction drove the temperature still higher in an unstable loop which resulted in the friction and temperature continually increasing at constant operating speed and pressure.

In other cases the clearance gap between the ring and the cylinder wall

was too large and sealing could not be established. Consequently, this concept was abandoned as impractical.

2.3 - Bonded Piston Ring Set

Functionally, the bonded rings are identical to the traditional split "pumping" piston rings which are employed as sets of two with maximum pressure in between.

The specific design of the compound rings addresses those issues derived from the very small axial thickness of these rings. In particular, achieving a good quality step joint ensuring that the low rigidity of the rings is not harmful to their proper operation, and good sealing of the back side of the ring are some of the main issures addressed by the design.

Other important features are the ability of the ring to undergo considerable wear with no adverse effect on the performance and simple, inexpensive construction of the ring and the piston.

The ring set assembly is shown schematically in Figure 2.4. The entire assembly fits into a single groove in the solid (one piece) piston. The two rings are separated by a spacer ring made of plastic which incorporates, on both its axial faces, radial leakage grooves which prevent these faces from sealing when the instantaneous cycle pressure is higher than the pressure between the rings. The spacer ring is open to allow installation in the groove of the one-piece piston.

At the back of each ring is a back-up rubber ring which provides sealing of the radial leak path at the step joint. The edges of the step joint are not radial lines, but are contoured so that at the outer diameter the edge is radial and at the inner diameter it is substantially tangential. This will prevent the rubber back-up ring from extruding into the slot after it has

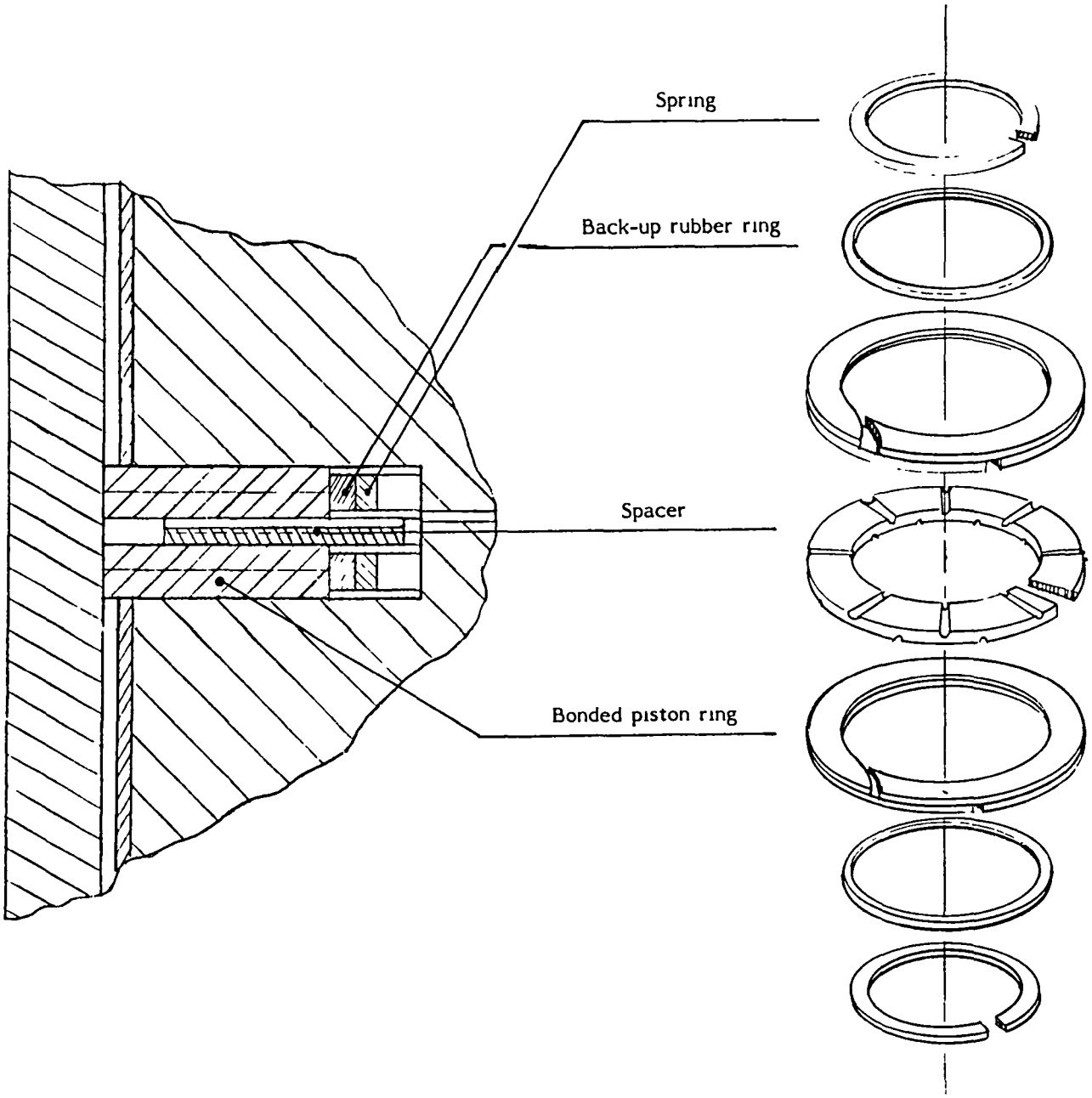

Figure 2.4

Bonded Piston Ring Set

opened due to wear as shown in Figure 2.5. This will permit the piston ring to accomodate a substantial amount of wear with no adverse effect on the performance.

Rulon tape is glued to the cylinder directly above and below the piston ring groove to prevent metal-to-metal contact between the piston and the cylinder as well as to prevent the thin piston rings from being extruded into the gap between the piston and the cylinder wall. Slanted leakage grooves in the Rulon tape, as shown in Figure 2.6, prevent it from participating in the sealing process. A high quality step joint is ensured by the method of fabrication of the bonded piston rings as shown in Figure 2.7.

To fabricate each bonded ring two identical closed rings are made from thin Rulon sheet and split with a contoured tool (step 1 in Figure 2.7). Glue is applied to one ring covering its axial face except for the part intended for the step joint which is left exposed. The other ring is glued to the first ring so that the splits are not alligned but, rather, span the step joint area (step 2 in Figure 2.7) yielding the finished compound ring. In production the rings with the contoured split could easily be stamped from thin Rulon sheets or cast in one piece.

The entire ring assembly, viz. the piston rings, spacer ring, back-up rings and springs, can be installed in a single groove in the solid, one-piece piston.

The space at the back of the ring assembly is connected to a convenient plenum to minimize the pressure fluctuation therein. A reasonably constant pressure (equal to the maximum cycle presure) in that space is essential for the proper operation of the ring set.

The configuration of the set of bonded piston rings which were tested differed from the one described above in that the edges of the step joint were

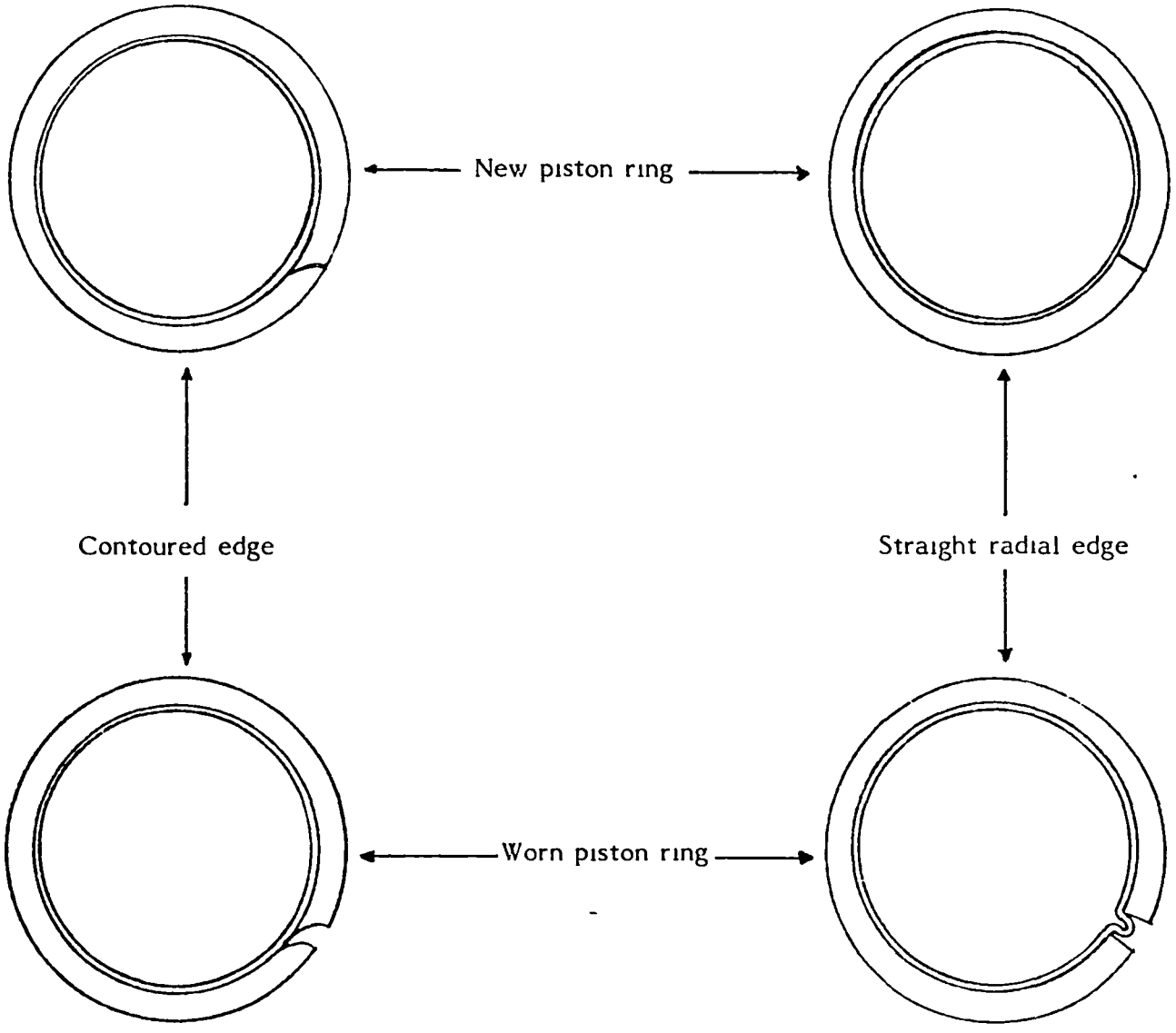

Figure 2.5 Advantages of Contoured Edge of Step Joint

After the piston ring has worn and the step joint opened up, the contoured edge of the step joint prevents the rubber back-up ring fron extruding into the opening.

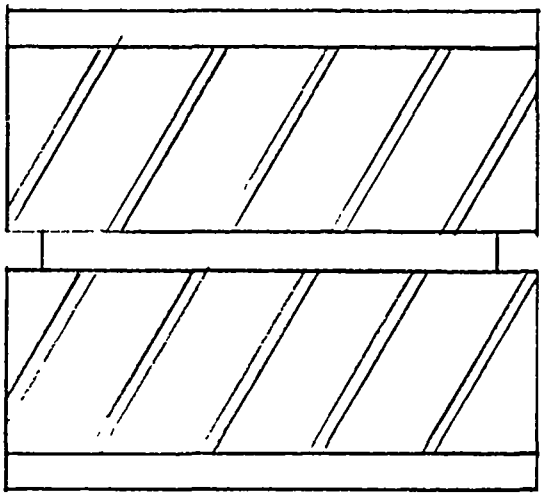

Figure 2.6

Slanted leakage grooves in Rulon tape bearing

Step 1

Two rings with contoured slots cut from thin sheet

Step 2

Adhesive (shaded areas) applied and rings are bonded with slots spanning the step joint area

A finished bonded piston ring

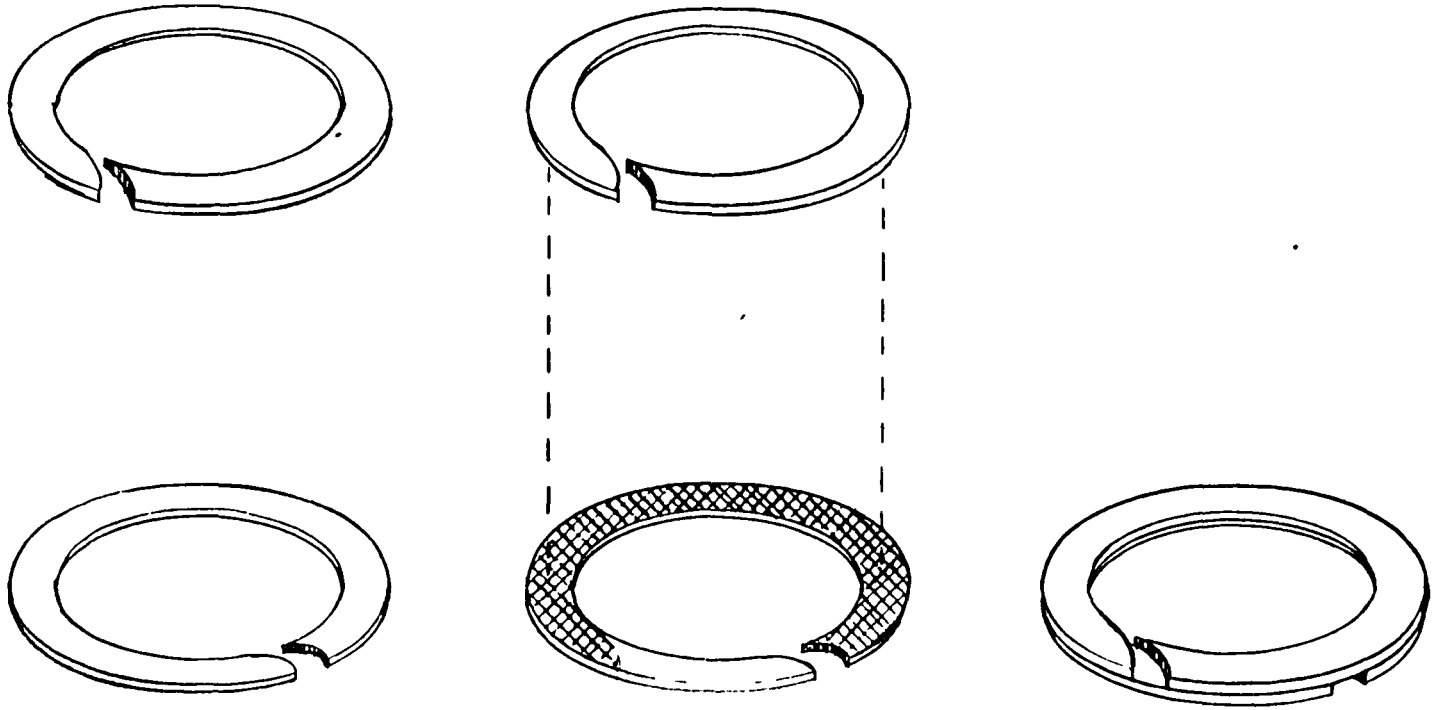

Figure 2.7

Method of fabrication of a bonded piston ring

radial rather than contoured and the grooved spacer ring was made of brass rather than plastic. A two-piece piston was used.

The piston was equipped with a dome, the internal volume of which was connected to the back of the piston ring groove providing a plenum of 38 cm^3.

In testing, the bonded piston rings exhibited low friction according to their small axial thickness. At the same time, the quality of the step joint and the positive sealing of its back side maintained relatively low leakage.

The bonded rings, in preliminary testing, were demonstrated to be a very promising concept which should be developed further.

2.4 - Description of the Test Rig

The test rig is shown schematically in Figure 2.8. A double acting, crank driven piston is compressing the helium gas in a sealed, blind cylinder. The variable volume above the piston is approximately equal to that below the piston. Piston rings mounted in the piston separate the two variable volumes, which undergo roughly harmonic pressure variation 180 degrees out of phase from each other.

The part of the cylinder which is swept by the piston ring is equipped with a water jacket. The water flow through the jacket is measured simply with a stop watch and graduated cylinder. The temperature difference between the inlet and outlet of the jacket is measured with a thermopile. In this way the energy input to the water jacket is indicated.

Thermocouples in the cylinder wall indicate the wall temperature of the two variable volumes.

Each of the variable volumes is equipped with two check valves, mounted in opposite directions, and with a restriction. These are connected to pressure

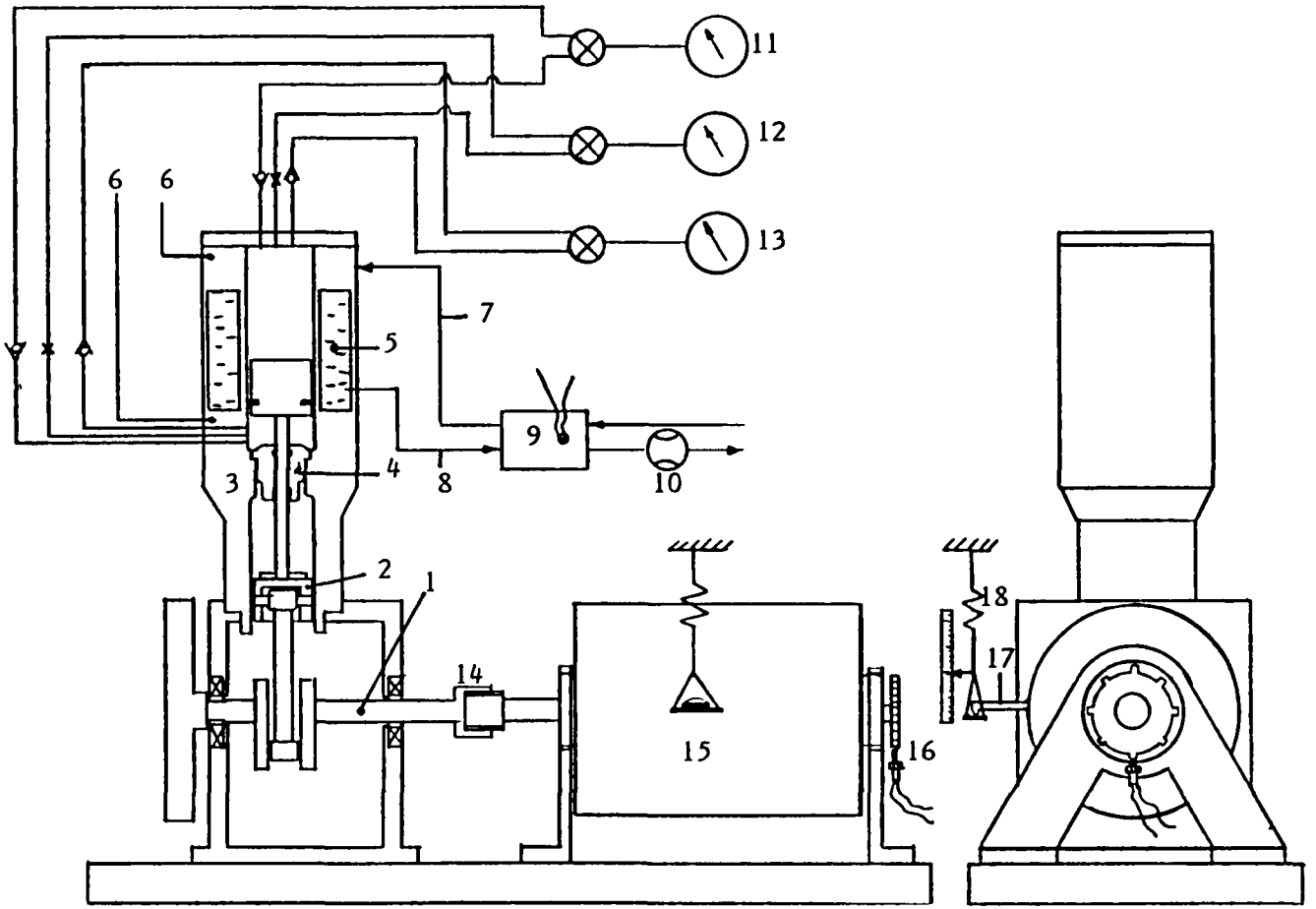

Figure 2.8

Variable Speed, Reciprocating Test Rig, Schematic

1) Crankshaft
2) Cross-head
3) Cylinder
4) Rod seal
5) Water jacket
6) Thermocouples
7) Water inlet
8) Water outlet
9) Thermopile
10) Water flow meter
11) Maximum pressure gage
12) Mean pressure gage
13) Minimum pressure gage
14) Coupling
15) Variable speed DC motor
16) Speed indicator
17) Torque arm
18) Balance

gages which indicate the maximum, minimum and mean pressure in each of the two volumes.

The rig is driven by a variable speed DC motor mounted on bearings such that its housing is free to rotate as shown in Figure 2.8. A torque arm attached to the housing is equipped with a knife edge which presses on the tray of a balance. The balance reading is proportional to the driving torque, the proportionality constant being the length of the torque arm. The speed is measured by a magnetic proximity sensor and cog wheel arrangement. The temperature of the lubricating oil supplied to the crank drive of the rig is maintained constant at 45°C by a thermostat controlled heated sump so that the effect of temperature on the drive friction through its effect on the oil viscosity is eliminated.

A layout drawing of the rig is shown in Figure 2.9. Figure 2.10 is a photograph of the rig.

In summary, the rig is instrumented to measure the following quantities:

- Maximum, minimum and mean pressure in each of the two variable volumes;
- Rotational speed of the rig;
- Mechanical energy input to the rig;
- Heat energy input to the water jacket; and
- Wall temperature of each variable volume

2.5 - Energy Flow in the Test Rig

At steady state, mechanical energy (W) per revolution supplied to the rig and measured by the balance, is converted in its entirety to heat. Four separate mechanisms facilitate this process:

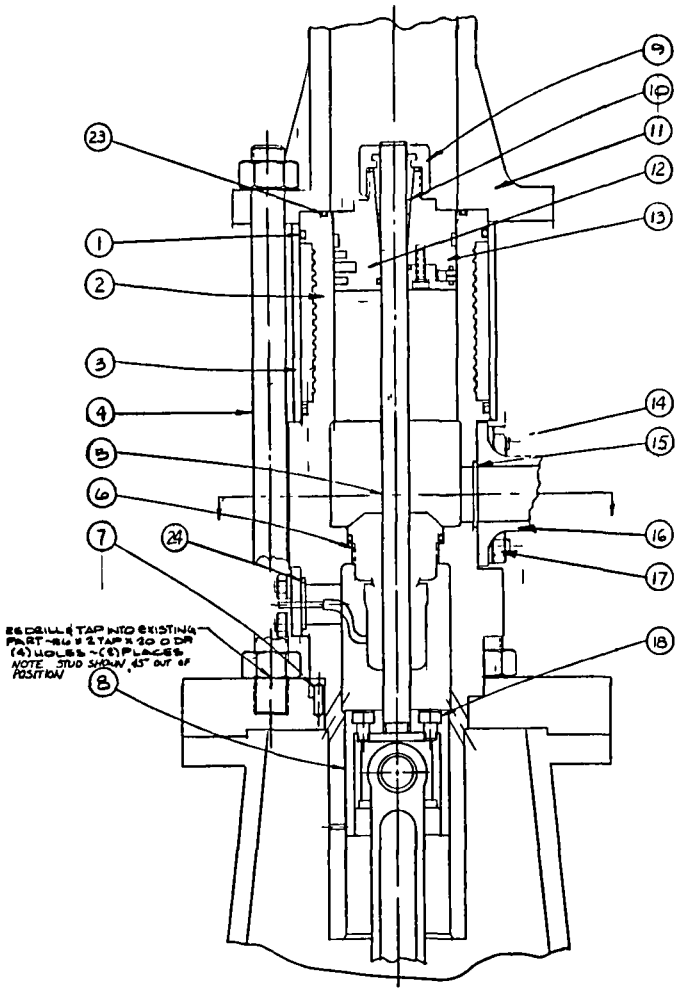

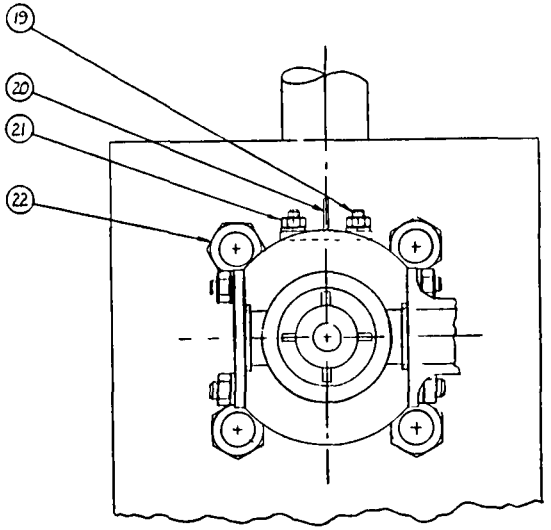

DET	AMT	DESCRIPTION	MAT'L
24	2	O RING 2-16	PUR
23	2	O-RING 2-114	PUR
22	8	M16×2 NUT	STD
21	8	M6×1 NUT	STD
20	2	P/N 60010	1020
19	8	M6×1 STUD 35 LG	STD
18	4	M6×1 SHCS 8 LG	STD
17	16	M8×1.25 NUT	STD
16	2	P/N 60009	1020
15	4	O RING 2-215	PUR
14	16	M8×1.25 STUDS 35 LG	STD
13	2	ASSY # 60008	—
12	2	ASSY # 60007	—
11	2	P/N 60006	ASTM 1374 TYP
10	2	UNIVERSAL ACME GR 8 COUPLET #30500 × 1" LG	PUR
9	2	UNIVERSAL ACME GR 8 NUT # 30250	PUR
8	2	P/N 60004	VAR
7	2	4 DIA × 10 LG ROLL PIN	PUR
6	2	ASSY # 10053	—
5	2	P/N 60005	NITRALLOY G
4	8	M6×2 STUD - 270 LG	PUR
3	2	#3/8 OD × .25W MODIFIED P/N 60006	CS 0.8.M TUBING
2	2	P/N 60001	AL 390
1	4	O-RING 2 236	PUR

Figure 2.9

RECIPROCATING TEST RIG

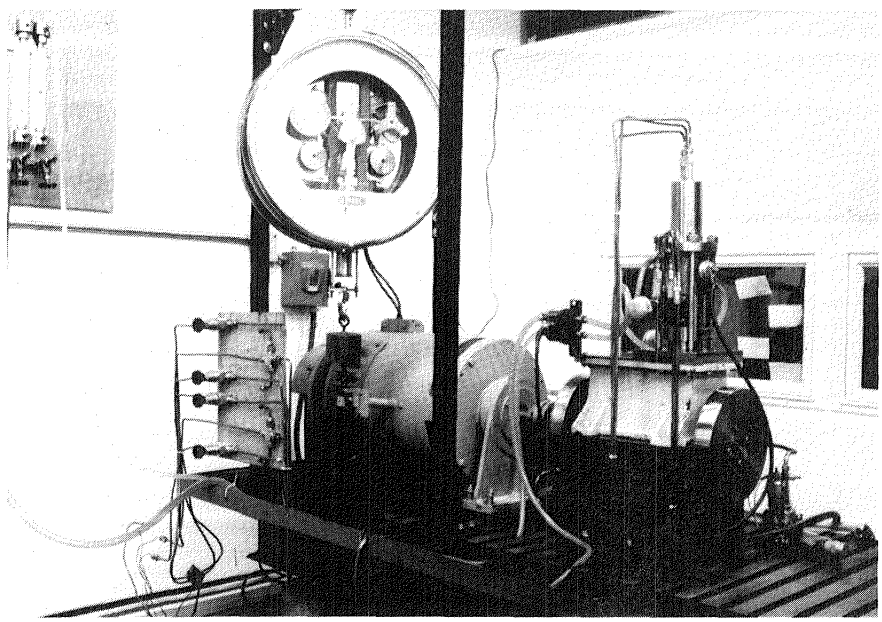

Figure 2.10

Variable Speed Reciprocating Rig

1) Mechanical friction in the crank drive mechanism (Q_o);

2) Piston ring friction (Q_f);

3) Piston ring leakage (Q_L); and

4) Hysteresis in the gas thermal boundary layer (Q_h).

Head developed in these processes is dissipated as follows:

1) Mechanical friction heat is dissipated by the lubrication system

2) Piston ring friction heat is disspated by the water jacket

3) Leakage and hysteresis heat is dissipated partly by radiation and convection from the cylinder wall and partly by the cooling jacket.

The above energy flow is summarized in Figure 2.11. It is important to note that the leakage loss (Q_L) is really composed of two separate effects: (Q_L) = Q_{Lp} + Q_{Lo}).

1) The phase shift effect (Q_{Lp}), caused by a phase shift between the volume variation and the bulk pressure variation, equally influences every infinitessimal volume of gas in the cylinder. It may be considered as a distributed volume source which transfers heat to the cylinder wall. Part of that heat is radiated and convested to the ambient and part is conducted to the water jacket.

2) The orifice effect (Q_{Lo}) dissipates heat locally at the piston ring by the frictional resistance of the gas leaking through the orifice.

In the test rig, analytical considerations (see Appendix I) indicate that the phase shift effect is about 40% smaller than the orifice effect. In an engine, however, the situation is completely reversed since the phase shift effect disturbs the principal process of energy conversion and thus accounts for a major loss whereas the ofifice effect is a relatively minor parasitic loss.

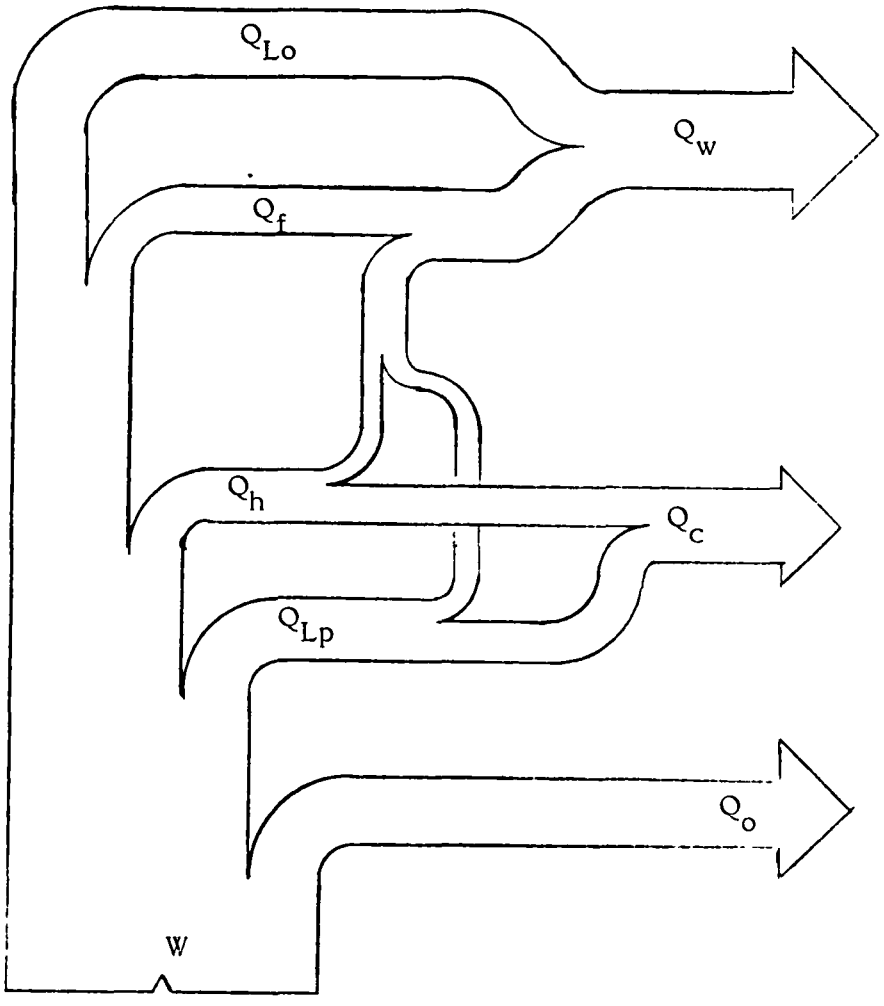

W	Work input (measured by balance)
Q_o	Heat dissipated by lubrication system
Q_{Lp}	Piston ring leakage heat by phase-shift effect
Q_{Lo}	Piston ring leakage heat by orifice effect
Q_h	Hysteresis heat
Q_f	Piston ring friction heat
Q_c	Total heat dissipated from uncooled cylinder wall
Q_w	Total heat dissipated by water jacket

Figure 2.11

Energy Flow Diagram for the Piston Ring Test Rig

For the tests described here the important fact is that the heat generated by the orifice effect is directly transmitted to the water jacket since it is generated locally at the ring. The heat generated by the phase shift effect can be regarded as emanating from a distributed volume source and is first transmitted to the cylinder wall from which a part is conducted to the water jacket and the balance convected and radiated to the surroundings.

The work input (W) is directly measured by the balance and the total heat dissipated by the water jacket (Q_w) is measured by measurement of the water flow and the temperature difference (ΔT) between the inlet and outlet of the jacket.

As long as the water jacket temperature and geometry stay constant the quantity ($Q_{Lp} + Q_h$) as well as the fraction (ϵ) of that quantity which is conducted to the water jacket are uniquely related to the temperature of the cylinder wall.

The relation between ($Q_{Lp} + Q_h$) and the cylinder wall temperature (T_c) was determined experimentally by placing a heating element inside the stationary rig cylinder, running water through the jacket, and measuring the cylinder wall temperature and the water jacket ΔT for various levels of electric heat input (Q_{in}). The results of these measurements are shown in Figure 2.12.

Since the purpose is to measure the friction loss (Q_f) and the leakage loss (Q_L) of the piston rings, and since the above measurements yield the following quantities:

$$Q_w = Q_f + Q_{Lo} + \epsilon\,(Q_{Lp} + Q_h) \quad ;$$

$$Q_{Lp} + Q_h \equiv Q_{vol} \quad ; \text{ and}$$

$$\epsilon = 1 - Q_c/(Q_{Lp} + Q_h)$$

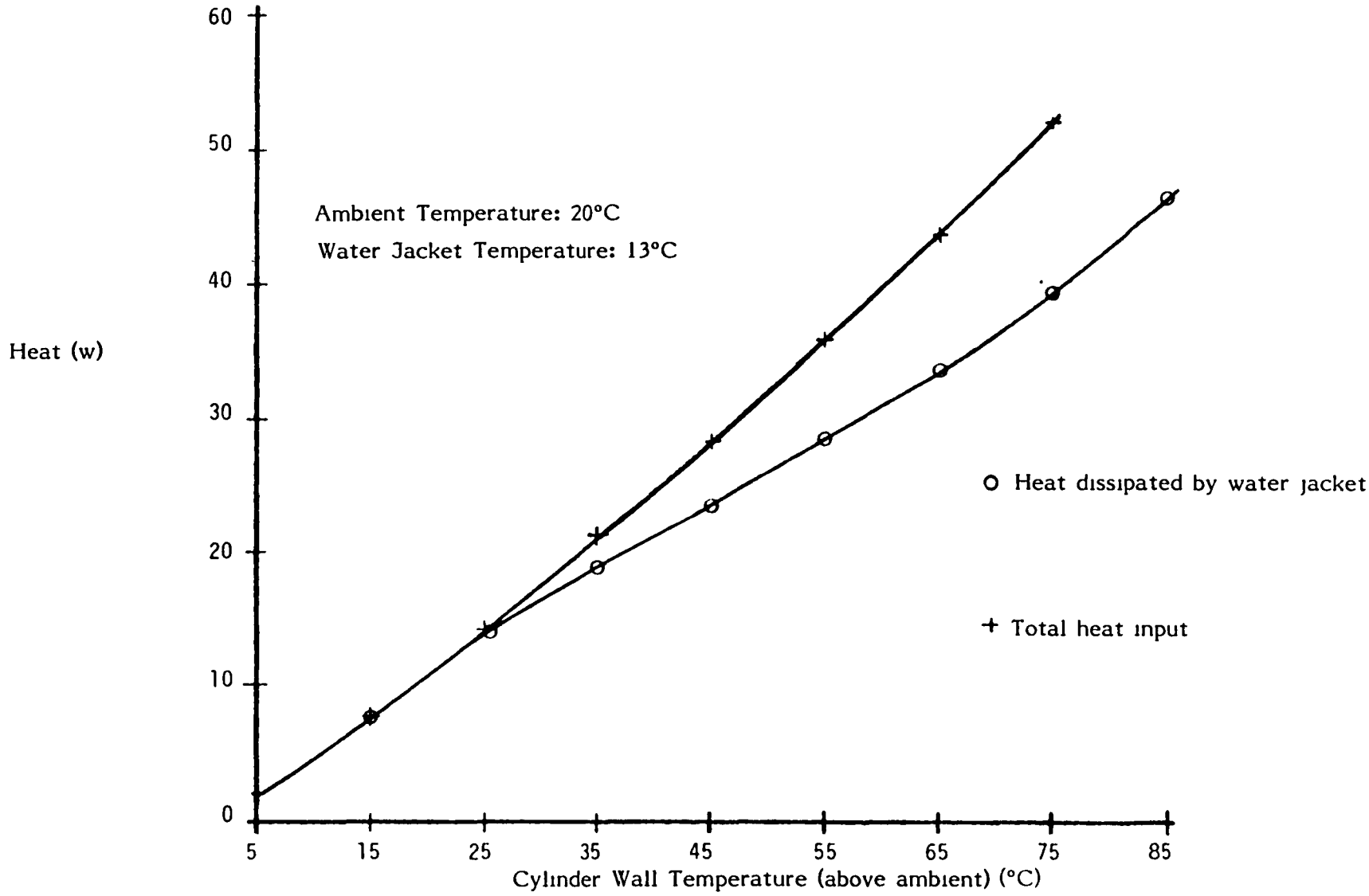

Figure 2.12

Dependence of the volume heat input and its fraction conducted to the water jacket on the cylinder wall temperature

we must be able to separate the contributions of friction, leakage, and hysteresis to the above quantities. Such separation is facilitated by the different influence of the speed on each of three losses:

- Piston ring friction heat loss per cycle is independent of the speed. (see Appendix II):
- Piston ring leakage heat loss per cycle is inversely proportional speed (see Appendix I);
- Hysteresis heat loss per cycle is inversely proportional to the square root of the speed (see, e.g. Ref. 1)

With Q_f , Q_L and Q_h known, the work input W, measured by the balance yields the drive friction (Q_o) as follows:

$$Q_o = W - Q_f - Q_L - Q_h$$

2.6 - Data Reduction for Piston Ring Performance

Data which was taken early in the program did not include coolant flow and temperature difference and did not include cylinder wall temperature. Therefore all the data which did include these measurements was used to characterize the drive losses (Q_o) which was then applied to the rest of the data. This method also increased the accuracy since the work input data indicated by the scale is more accurate than the water jacket data.

According to Section 2.5 above the following quantities were measured:

$$Q_w = Q_f + Q_{Lo} + \epsilon\,(Q_{Lp} + Q_h) \qquad (2.1)$$

$$Q_{vol} = Q_{Lp} + Q_h \qquad (2.2)$$

$$\epsilon = 1 - Q_c/Q_{vol} \qquad (2.3)$$

$$W = Q_o + Q_f + Q_{Lo} + Q_{Lp} + Q_h \qquad (2.4)$$

Solution of the above four equations for Q_o in terms of the measured quantities on the left hand side of the equations yields:

$$Q_o = W - Q_w - (1 - \epsilon)\, Q_{vol} \tag{2.5}$$

A drive friction coefficient (f_d) was defined as follows:

$$f_d = \frac{Q_o}{\pi\, d_b\, A_p\, p_m} \tag{2.6}$$

where

d_b is the main bearings radius;

A_p is the piston area; and

P_m is the mean pressure

Hydrodynamic lubrication theory stipulates a linear relation between the friction coefficient f_o per 2.6 above and the non-dimensional parameter S defined as follows:

$$S = \mu \frac{\omega}{p_m} \tag{2.7}$$

where

μ is the dynamic viscosity of the oil; and

ω is the angular speed

Since the drive friction is independent of the rings used all the available data (34 data points of three different rings) were used to fit a linear curve (by the least squares method) to the relation betwen f_d and S.

The data and the fitted curve is shown in Figure 2.13. Q_o is now given fairly accurately as a function of speed (ω) and mean pressure (p_m).

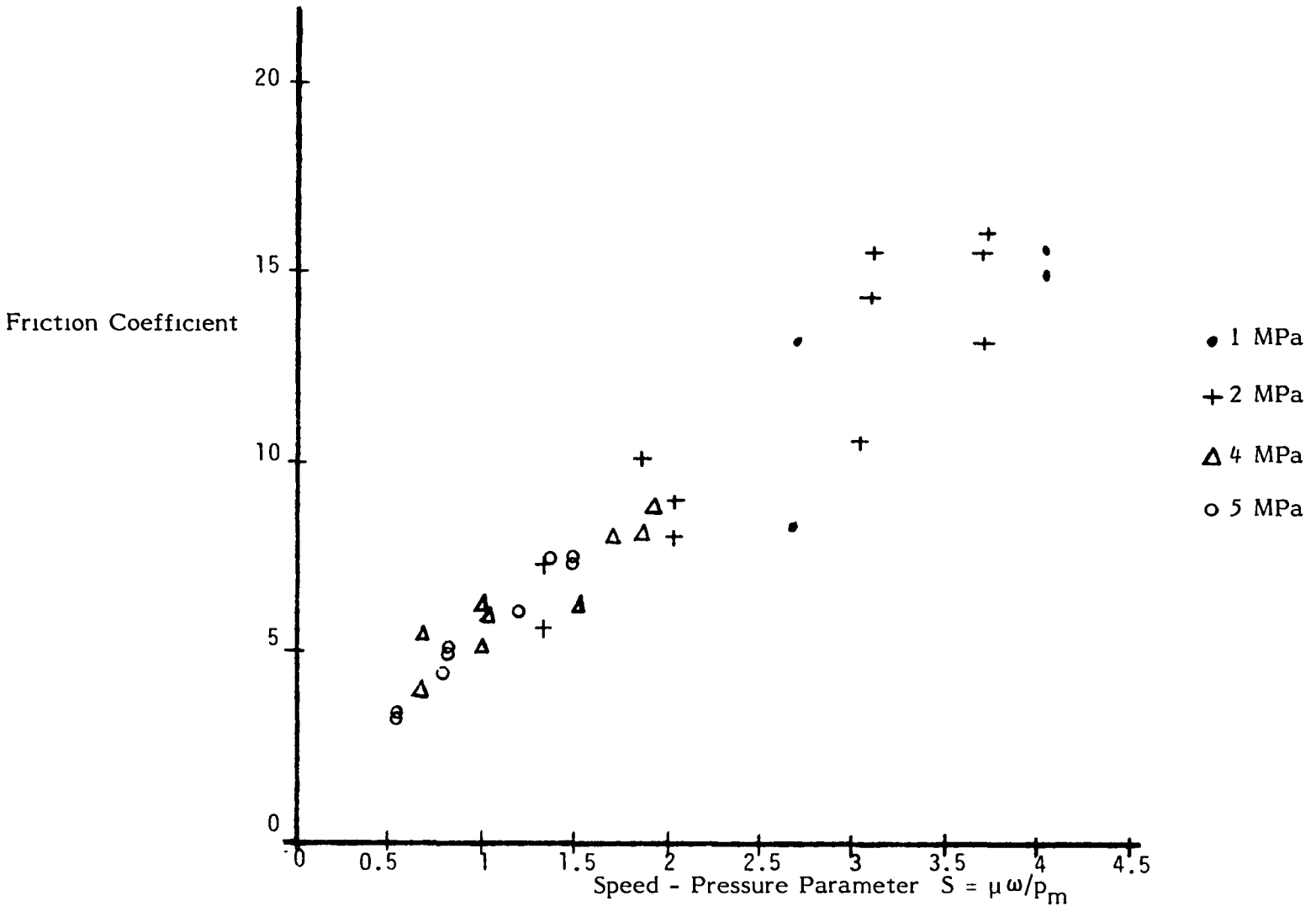

Figure 2.13

Drive Coefficient vs. Speed-Pressure Parameter

The fitted curve is:

$$f_d = \alpha_o + \alpha_1 S \tag{2.8}$$

substitution of 2.6 and 2.7 in 2.8 yields:

$$\frac{Q_o}{\pi d_b A_p p_m} = \alpha_1 \mu \frac{\omega}{p_m} + \alpha_o \tag{2.9}$$

and rearranging:

$$Q_o = \pi d_b A_p (\alpha_o p_m + \alpha_1 \mu \omega) \tag{2.10}$$

This was now applied to all the data including such measurements where coolant and cylinder wall temperature data were not available. The drive losses (Q_o) per 2.10 above was subtracted from the measured work input (W) to yield a quantity ($W - Q_o$) which according to Section 2.5 above is made up of the following:

$$(W - Q_o) = Q_f + Q_{Lo} + Q_{Lp} + Q_u = C_f + (C_{Lo} + C_{Lp})/\omega + C_h/\sqrt{\omega} \tag{2.11}$$

Least squares were used to fit the curve on the extreme right hand side of 2.11 to each set of ($W - Q_o$) quantities taken for a particular ring at constant mean pressure.

2.7 - Results

The results of the performance measurements of the four sets of piston rings are presented and discussed in this section. Tables 2.1 through 2.4 list the various losses for all four sets of rings at different speeds and pressures. The data is further reduced to achieve a clearer indication of trends

Table 2.1

Summary of Energy Flow per Cycle - Ring Set #1

Mean Pressure (MPa)

	1	2	3	4	5	6
Q_f (all speeds)		4.14		5.3		5.63
Speed (RPM)		750		750		750
Q_L		20.7		33.35		45.3
Q_d		6.24		7.74		9.21
Q_w		8.54		38.56		50.97
W		31.10		46.30		60.19
Speed (RPM)		1125		1125		1125
Q_L		13.80		22.23		30.20
Q_d		8.54		10.12		11.70
Q_w		17.92		27.80		35.70
W		26.46		37.02		47.99
Speed (RPM)		1500		1500		1500
Q_L		10.35		16.68		22.65
Q_d		10.63		12.38		14.62
Q_w		14.51		21.79		28.37
W		25.13		34.17		42.99
Speed (RPM)						
Q_L						
Q_d						
Q_w						
W						

Where: Q_f = Piston Ring Friction - Joules

Q_L = Piston Ring Phase Shift plus Orifice Leakage Effects - Joules

Q_d = Crank Drive Friction - Joules

Q_w = Heat Dissipated by Water Jacket - Joules

W = Mechanical Energy Input - Joules

Table 2.2

Summary of Energy Flow per Cycle - Ring Set #4

	Mean Pressure (MPa)					
	1	2	3	4	5	6
Q_f (all speeds)	.47	1.77		4.47	6.93	
Speed (RPM)	794	790		785	805	
Q_L	6.35	8.87		11.10	10.10	
Q_d	5.53	6.63		7.99	9.14	
Q_w	6.70	10.13		15.37	16.77	
W	12.24	16.76		23.37	25.90	
Speed (RPM)	1197	1205		1196	1194	
Q_L	4.21	5.81		7.28	6.79	
Q_d	7.89	8.77		10.33	11.70	
Q_w	5.00	7.76		12.26	13.70	
W	12.90	16.54		22.60	25.35	
Speed (RPM)	1810	1805		1805	1815	
Q_L	2.79	3.88		4.83	4.46	
Q_d	11.46	12.49		14.03	14.62	
Q_w	1.22	5.27		8.90	11.17	
W	12.68	17.75		22.92	25.79	
Speed (RPM)	2210	2200		2209	2212	
Q_L	2.28	3.19		3.94	3.66	
Q_d	14.14	14.62		16.18	17.30	
Q_w	4.38	5.48		9.60	10.69	
W	18.52	20.10		25.79	27.99	

Where: Q_f = Piston Ring Friction - Joules

Q_L = Piston Ring Phase Shift plus Orifice Leakage Effects - Joules

Q_d = Crank Drive Friction - Joules

Q_w = Heat Dissipated by Water Jacket - Joules

W = Mechanical Energy Input - Joules

Table 2.3

Summary of Energy Flow per Cycle - Ring Set #2

	Mean Pressure (MPa)					
	1	2	3	4	5	6
Q_f (all speeds)	2.86	3.95	6.94	7.89	12.46	
Speed (RPM)	797	790	812	810	810	
Q_L	5.43	8.69	8.68	10.26	7.37	
Q_d	5.61	6.34	7.31	8.58	9.50	
Q_w	8.28	12.51	15.18	17.88	19.60	
W	13.89	18.85	22.49	26.46	29.10	
Speed (RPM)	1196	1100	1174	1184	1213	
Q_L	3.61	6.24	6.00	7.02	4.92	
Q_d	7.95	8.09	9.36	10.33	11.70	
Q_w	6.47	10.43	15.18	15.46	17.84	
W	14.42	18.52	23.15	25.79	29.54	
Speed (RPM)		1830	2012	2025	2031	
Q_L		3.75	3.50	4.11	2.94	
Q_d		12.58	14.62	15.60	15.84	
Q_w		7.71	10.51	11.90	15.69	
W		20.28	25.13	27.56	31.53	
Speed (RPM)		2190	2220	2197	2217	
Q_L		3.13	3.17	3.78	2.69	
Q_d		14.62	15.94	16.57	17.55	
Q_w		6.98	9.64	11.43	14.64	
W		21.61	25.57	27.99	32.20	

Where: Q_f = Piston Ring Friction - Joules

Q_L = Piston Ring Phase Shift plus Orifice Leakage Effects - Joules

Q_d = Crank Drive Friction - Joules

Q_w = Heat Dissipated by Water Jacket - Joules

W = Mechanical Energy Input - Joules

Table 2.4

Summary of Energy Flow per Cycle - Ring Set #3

	Mean Pressure (MPa)					
	1	2	3	4	5	6
Q_f (all speeds)	2.44	5.10	6.81	9.11	14.5	12.72
Speed (RPM)	800	800	800	800	800	800
Q_L	4.04	5.27	6.15	6.22	2.47	7.677
Q_d	5.61	6.24	7.60	7.80	9.26	9.80
Q_w	6.52	10.30	12.68	15.13	16.97	19.97
W	12.13	16.54	20.28	22.98	26.23	29.76
Speed (RPM)	1200	1200	1200	1200	1200	1200
Q_L	2.69	3.51	4.10	4.15	1.65	5.12
Q_d	7.97	8.87	9.43	10.43	10.97	11.70
Q_w	5.04	8.77	11.50	13.60	16.15	18.73
W	13.00	17.64	20.94	24.00	27.12	30.29
Speed (RPM)	2000	2000	2000	2000		
Q_L	1.62	2.11	2.46	2.49		
Q_d	12.67	13.45	14.55	14.62		
Q_w	4.30	7.27	9.26	12.27		
W	17.00	20.72	23.81	26.90		
Speed (RPM)	2225	2225	2225	2225		2225
Q_L	1.45	1.89	2.21	2.24		2.76
Q_d	14.14	14.96	15.99	16.57		18.29
Q_w	3.70	6.86	8.72	10.54		15.01
W	17.90	21.83	24.69	27.12		33.29

Where: Q_f = Piston Ring Friction - Joules

Q_L = Piston Ring Phase Shift plus Orifice Leakage Effects - Joules

Q_d = Crank Drive Friction - Joules

Q_w = Heat Dissipated by Water Jacket - Joules

W = Mechanical Energy Input - Joules

as follows:

2.7.1 Friction - The friction data was reduced using equation II-8 from Appendix II to glean the friction coefficient f:

$$f = \frac{Q_f}{2 \pi D S h p_m n (\Delta V/V_m)}$$

If the friction mechanism is indeed the one modelled in Appendix II then the friction coefficient f is only a function of the material.

Figure 2.14 shows the friction coeffecient of all rings plotted versus the mean pressure p_m. There is a substantial spread of the data about an average value of 0.17 which is somewhat higher than that (0.15) commonly specified in the literature. The spread of the data appears to be random and does not show any particular trend. Both the data spread and the slightly higher average value may be explained by the fact that the hysteresis losses, being of the same order of magnitude as the error in the measurement, are partially included in the friction and leakage losses in a random manner. Since leakage loss in the rig is much higher than the friction loss the hysteresis error influence on the latter is much higher than on the former. The conclusion is that the friction loss is proportional to the axial thickness (h) of the rings and, more generally, that the friction mechanism is correctly modelled in Appendix II.

2.7.2 Leakage - The leakage data was reduced to eliminate the influence of speed using equation

$$Q_L = C_L/\omega$$

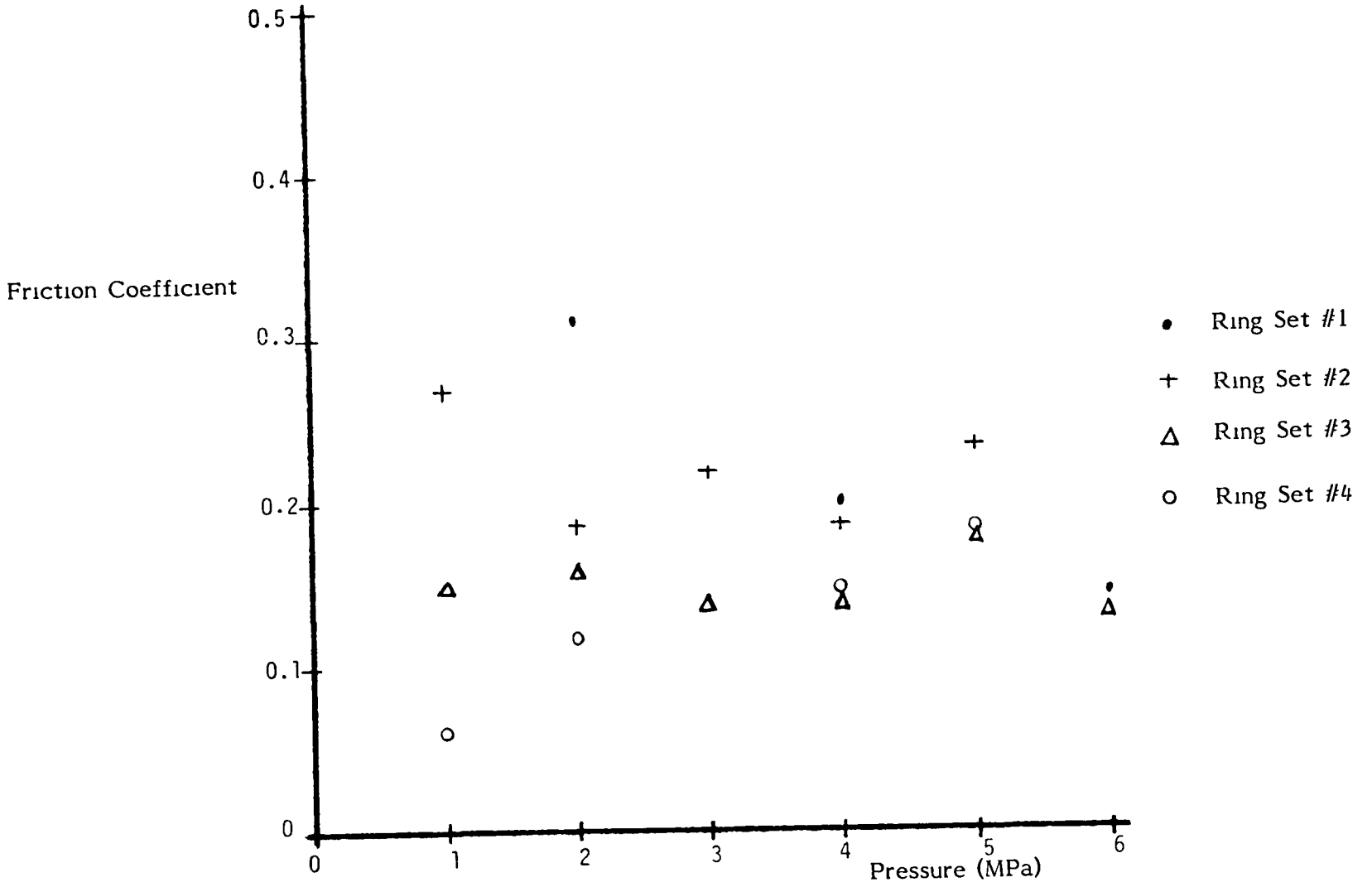

Figure 2.14

Piston Ring Coefficient vs. Mean Pressure

The "leakage coefficient" C_L is a monotonically increasing function of the mean pressure (linear for laminar restriction) the slope of which is inversely proportional to the restriction of the ring. Physically, C_L is proportional to the leakage power loss and its units are those of power:

$$C_L = 2\pi \frac{dQ_L}{dt}$$

Figure 2.15 shows the behavior of the coefficient C_L with pressure for the four sets of rings.

The most striking trend exhibited by Figure 2.15 is the large difference between the leakage of Ring Set #1 (the set with untreated surfaces of the step joints) and that of all other ring sets.

This clearly demonstrated that it is the quality of the step joint which exerts the most influence on the leakage characteristics of piston rings. Comparison of the data of Ring Sets # 2, 3 and 4 among themselves indicate the following:

- Ring set # 3 which has the largest axial thickness exhibits somewhat lower leakage than that of the other two sets (about 30% lower).
- Ring sets # 2 and 4 exhibit practically the same leakage
- Except for the reading at 5 MPa the data shows relatively little scatter and generally exhibits a linear trend in the pressure influence modified by a certain "flattening" at higher pressure indicating the presence of some turbulent effects on the leakage mechanism.

2.7.3 Comparison of Orifice Effects to Phase Shift Effects - Strictly theoretical consideration (see Appendix I) indicate that, for both laminar and

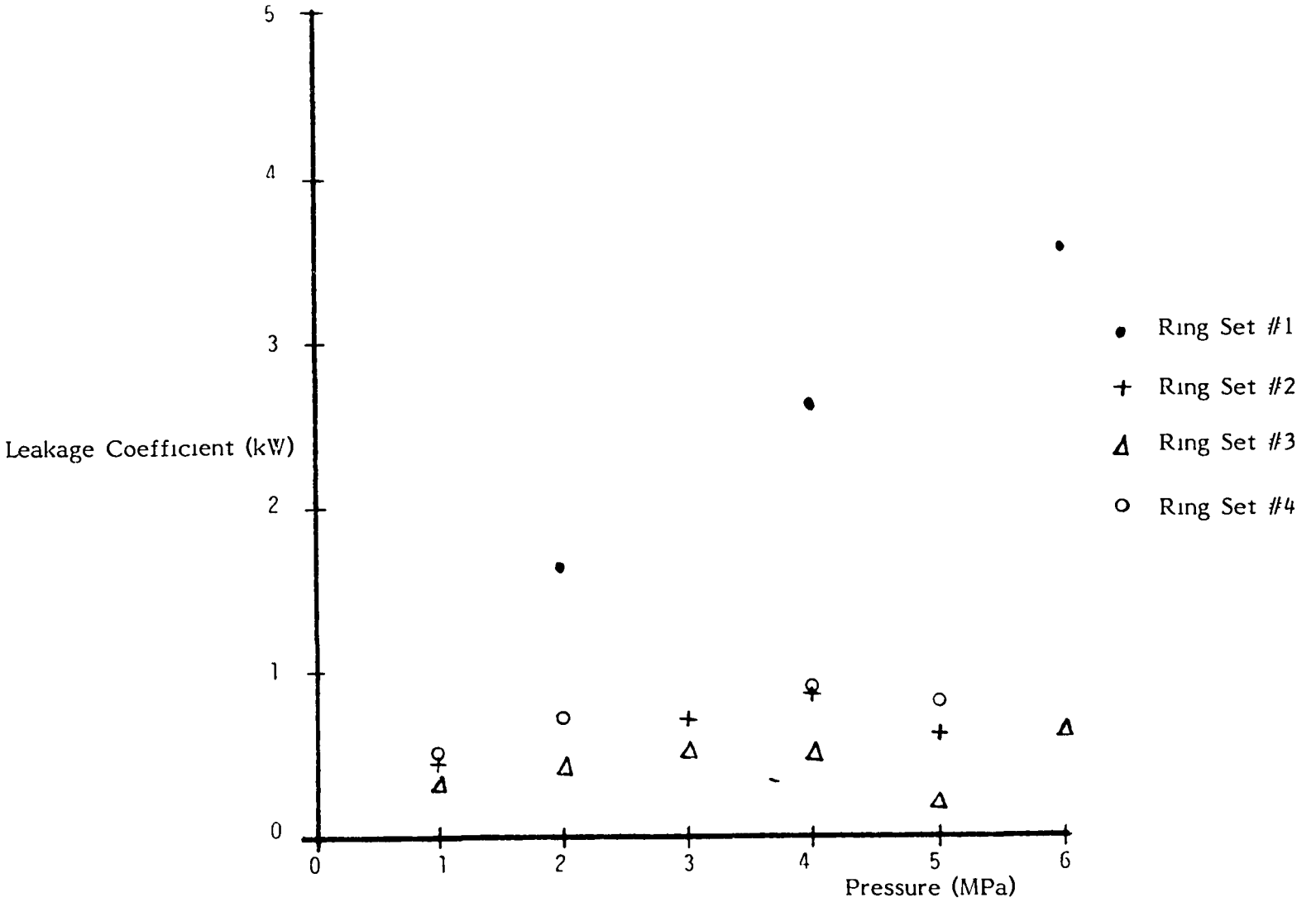

Figure 2.15

Piston Ring Leakage Coefficient vs. Mean Pressure

Table 2.5

Ratios of Orifice to Phase-Shift Leakage Effects

Mean Pressure (MPa)	Nominal Speed (RPM)	Q_{Lo}/Q_{Lp} for Ring Set #2	#4
1	800	1.09	1.37
1	1200	1.51	0.83
1	1800	0.73	0.81
1	2200	1.05	1.69
2	800	2.05	1.54
2	1200	1.78	1.37
2	1800	1.68	1.11
2	2200	2.41	1.47
4	800	1.33	2.07
4	1200	1.20	1.90
4	1800	1.17	1.84
4	2200	1.52	1.69
5	800	1.74	1.06
5	1200	1.72	1.06
5	1800	1.39	1.15
5	2200	2.05	1.23
Average Q_{Lo}/Q_{Lp}		1.53	1.38
Combined Average		1.46	

turbulent resistance, the ratio of the orifice effect power loss to the phase-shift effect power loss (Q_{Lo}/Q_{Lp}) is equal to the polytropic constant (n) of the compression and expansion processes.

For such rings where coolant and cylinder wall temperature were available (sets # 2 and 4) the data was reduced per Section 2.5 above to separate the above two leakage effects and indicate the ratio.

The results, tabulated in Table 2.5, show that, within the error of the measurement, the average ratio 1.46 (1.38 and 1.53 for Ring Sets # 4 and 2 respectively).

The polytropic constant is expected to be somewhat lower than the 1.67 characterizing purely adiabatic processes for the monoatomic helium, since some heat exchange with the ambience does occur. The average result of 1.46 is entirely reasonable and indicates that the data and the data reduction method do reflect the real physcial processes which occur in the testing.

2.7.4 Accuracy and Data Spread - Some indication of the accuracy of the data is afforded by comparing the actual data points indicating the total friction leakage and hysteresis loss (Q_{act}) to the values provided by the curve fitted to the data ($Q_{fit} = C_f + C_L/\omega$). The ratio ($Q_{act}/Q_{fit}$) is plotted versus speed and pressure for each set of rings and shown in Figures 2.16 through 2.19.

The following observations may be made:

- By and large, no trend can be distinguished in the influence of pressure and speed on the data spread.
- The data spread of Ring Set # 1 is extemely small (± 1% max.). This is because the total loss (particularly leakage) is so large. Results for Ring Set #1 are thus very accurate and reliable.

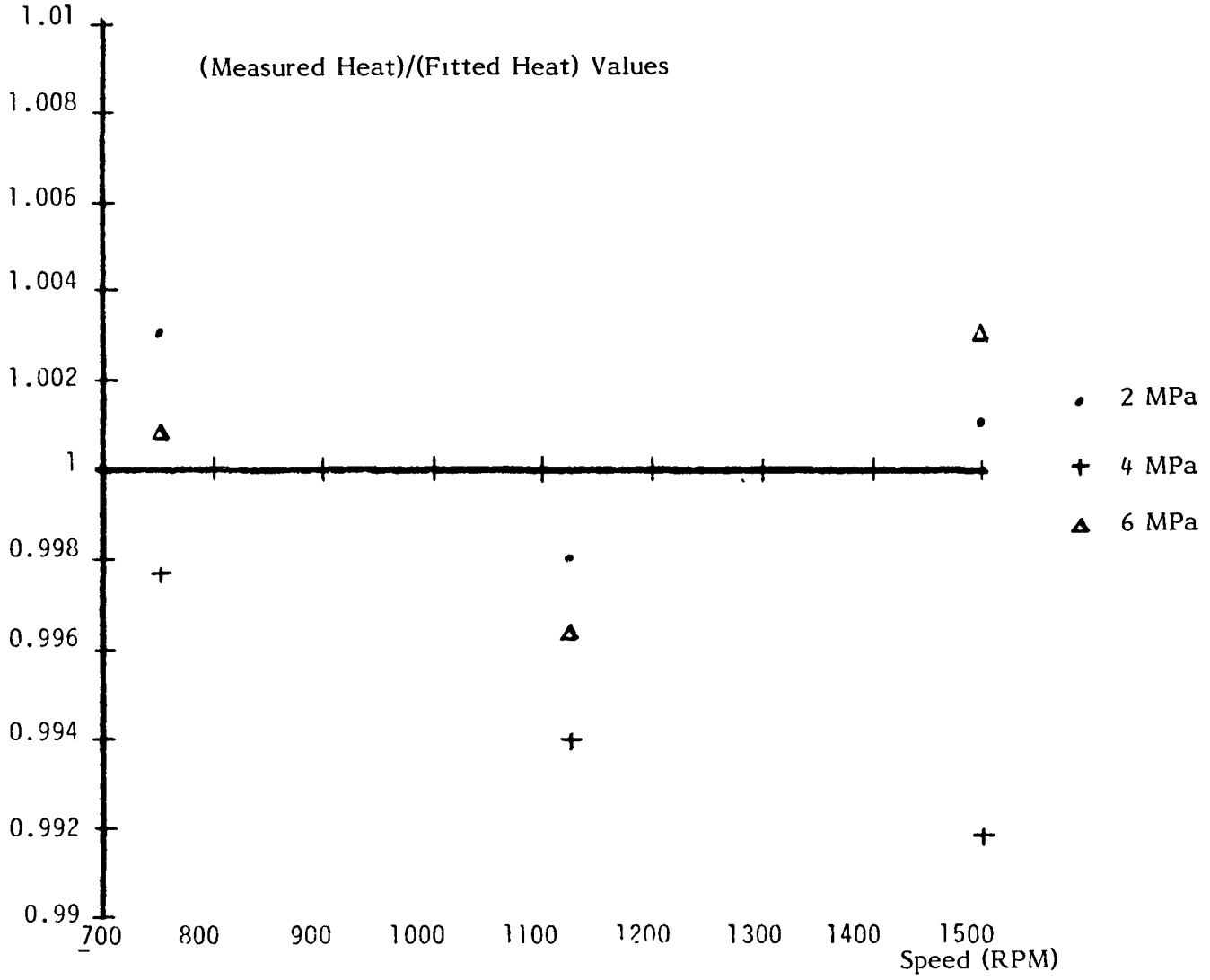

Figure 2.16

Quality of Curve Fit to Measured Data - Ring Set #1

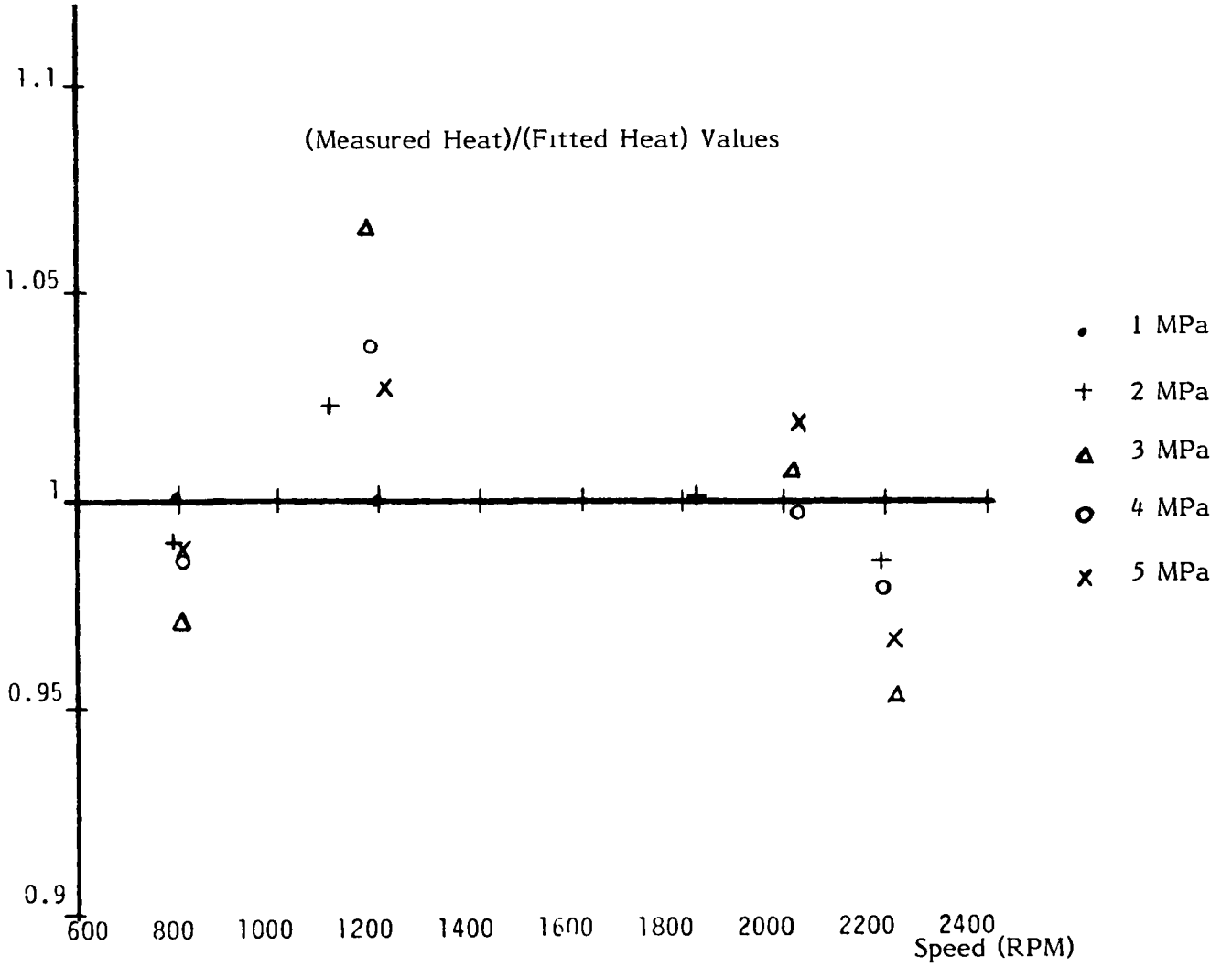

Figure 2.17

Quality of Curve Fit to Measured Data - Ring Set #2

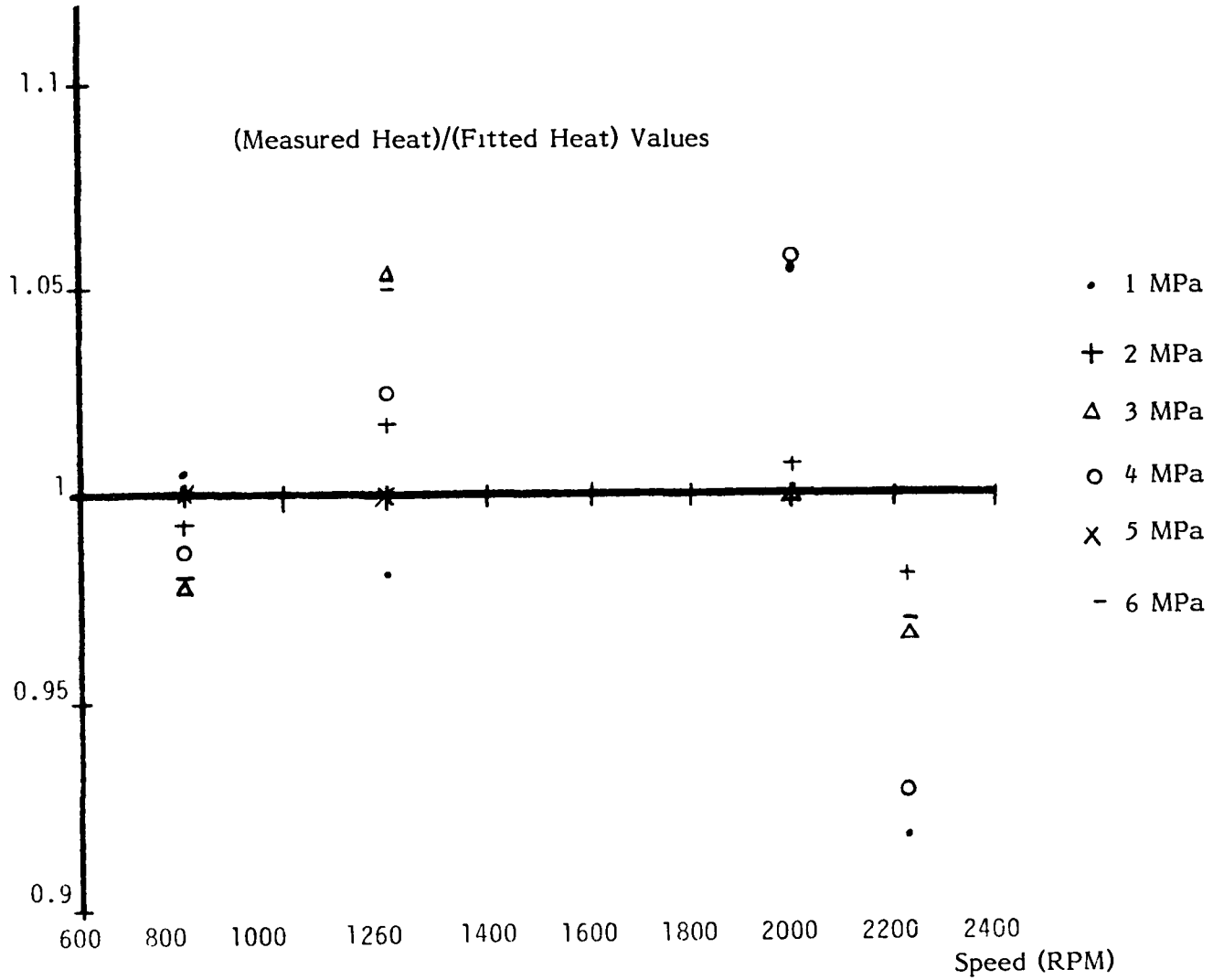

Figure 2.18

Quality of Curve Fit to Measured Data - Ring Set #3

SECTION 3 - RECIPROCATING ROD SEAL

3.1 Introduction and Summary

The Stirling engine concept which has been developed at Stirling Thermal Motors, Inc. involves a variable swashplate drive. Power control is accomplished by means of piston stroke variation affected by changing the swashplate angle. The mean cycle pressure in the engine thus remains constant at all operating conditions.

This makes it possible to maintain the crankcase at mean cycle pressure and thus relax the functional requirements of the reciprocating rod seal so that they are reduced to the following two:

- isolating the varying cycle pressure from the constant crankcase pressure; and
- preventing oil, present in the crankcase, from penetrating the thermodynamic cycles.

The first of these two functions is readily accomplished with a cap seal which is a Rulon (or similar thermoplastic material) ring backed up by an O-ring mounted around the piston rod.

Regarding the prevention of crankcase oil from penetrating into the cycles, previous experience with asymmetrically loaded scrapers made of babbit, or a similar soft metal, yielded very good results provided there was no clearance between the scraper and the rod.

Lateral motion of the rod, due to normal manufacturing tolerances effecting the cross-head clearance, necessarily causes clearance between the scraper and the rod to appear since the rod will wear down the babbit. This will cause the scraper to cease functioning properly after a short time of

- Ring Sets # 2 and 3 exhibit similar data spread of about 6%
- Ring Set # 4 exhibit the largest spread of 14% and also show an unexpected influence of pressure (a steady increase in the spread from 7% at 1MPa to 14% at 3 MPa and abrupt recduction to 2% at 4MPa). Data for this ring set is the least accurate and reliable and should be considered merely as preliminary indication of performance.

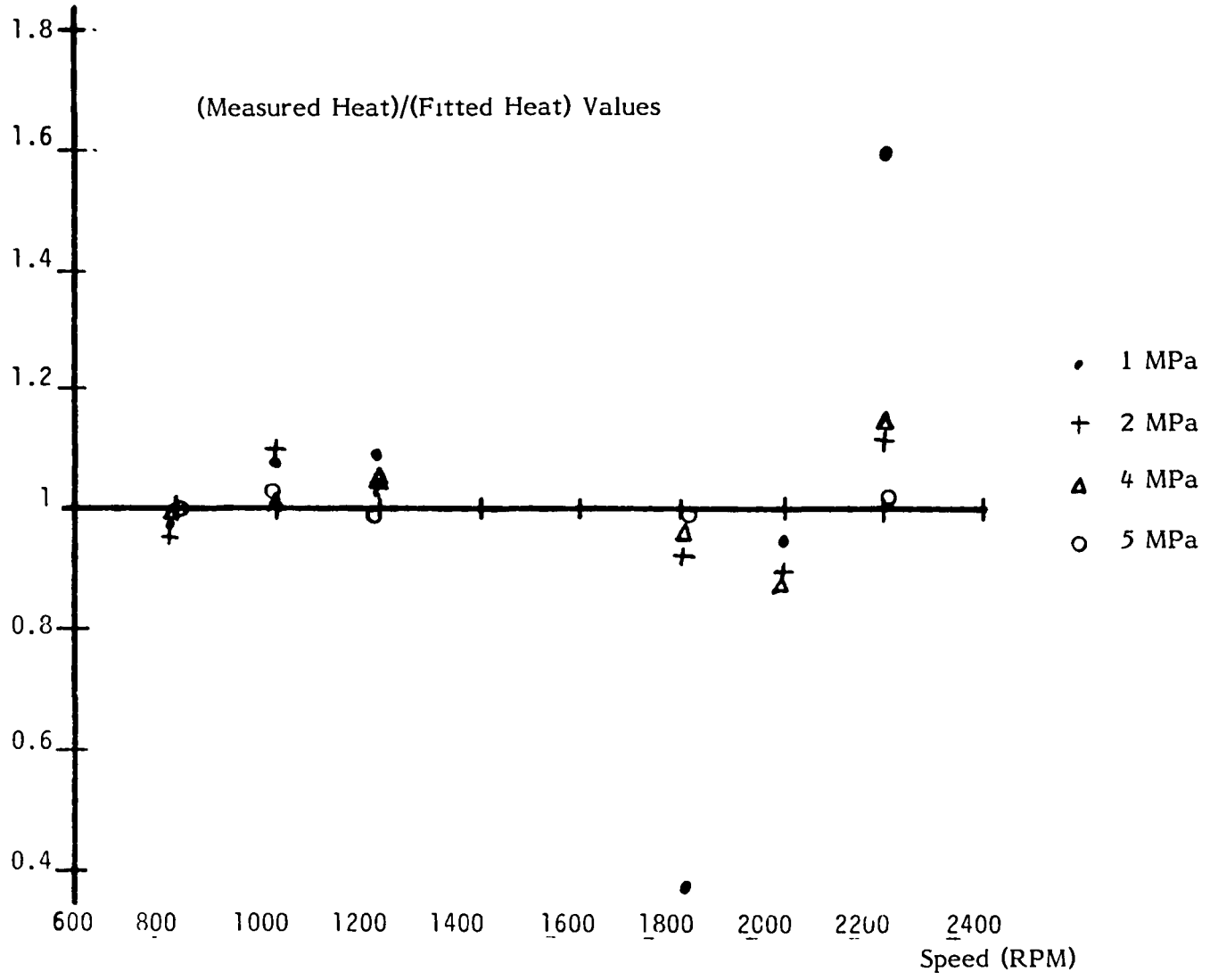

Figure 2.19

Quality of Curve Fit to Measured Data - Ring Set #4

operation.

To address this problem, Stirling Thermal Motors, Inc. has designed a compliant housing. The scraper is mounted to the compliant housing and is forced against the rod by a crown spring also mounted to the compliant housing. The entire assembly can move laterally with the piston rod without any appreciable force exerted on the scraper due to such motion.

The cap seal is also mounted in the compliant housing and follows the lateral motion of the rod.

The compliant housing is made of nylon. Its convoluted geometry makes it rigid axially and compliant laterally. The design is described in detail in Section 3.2 below.

The experimental assessment of the rod seal, hereunder, was aimed at the following two objectives:

- Assess seal endurance under design conditions, viz. with no pressure difference across the seal but with an appreciable lateral motion of the rod; and
- Assess much of the applicability of the seal as a containment seal for the gas as well as an oil scraper.

Endurance testing was performed at constant speed of 1800 RPM with atmospheric pressure on both sides of the seal and with lateral motion of the rod of an amplitude of 60 μm. By July 8, 1985, the seal has completed 6750 hours of operation without any failure and with no degradation of performance. During the entire test, frequent visual inspections discovered no oil at all above the seal. (There was one problem at about 400 hours which was specific to the test rig and does not indicate an inherent seal problem. This is described in Section 3.3 below).

These results are very encouraging and indicate the adequacy of the rod seal and the compliant housing to engines with a pressurized crankcase.

As a containment seal, with mean pressure difference across, the rod seal with the compliant housing did not perform very well. The following problems were identified:

- The low tensile strength of the nylon housing caused it to break under a pressure difference of 8 MPa across it.
- Skewed deformation of the nylon housing under pressure, due to some deviation from axial symmetry, induced plastic deformation of the soft babbit scraper. When the pressure was reduced this plastic deformation gave rise to some geometric incompatibility which prevented the seal from sealing oil.

In order to address these problems it is felt that a new compliant housing design is needed, such that will retain the compliance but will add significant tensile strength. In addition, the elastic limit of the scraper element itself should be increased. This may be accomplished by using a stronger metal, possibly plated with a layer of softer metal.

3.2 Rod Seal Design

An assembly drawing of the scraper rod seal is shown in Figure 3.1. The scraper (1) is made of tin babbit (ASTM 3) and is loaded against the rod by a crown spring (2) which exerts an even pressure on the sealing edge through a square rubber ring (3). The square ring (3) is retained between the scraper housing (4) and the spacer (5), and thus also seals the OD of the scraper (1). All the above components are mounted in the scraper body (6) which threads onto the compliant nylon housing (7) which also contains the cap seal (8). The

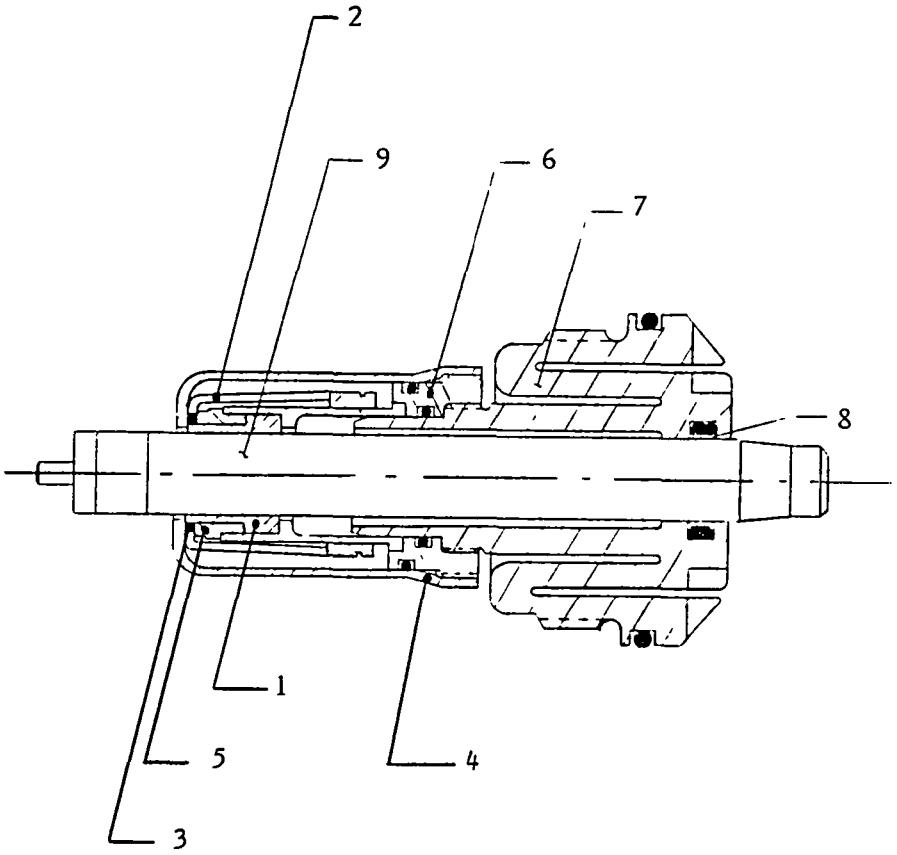

Figure 3.1

Scraper Rod Seal Assembly

1) Scraper (ASTM3 tin babbit)
2) Crown spring
3) Square rubber ring
4) Scraper housing
5) Spacer
6) Scraper body
7) Compliant housing (Nylon)
8) Cap seal (Rulon LD)
9) Assembly pilot (replacing piston rod)

compliant housing (7), in turn is threaded to the engine block. Photographs of the assembly and two stages of disassembly are shown in Figures 3.2, 3.3 and 3.4. The scraper itself is shown in Figure 3.5, and the crown spring in Figure 3.6.

3.3 Description of the Tests

The endurance test was performed on a reciprocating rig, shown in Figure 3.7, which was operated without a piston in order to deprive the rod from guidance. The space above the scraper assembly was open to the atmosphere and equipped, right above the seal, with inspection ports. The space below the seal, on the crankcase side, is also at atmospheric pressure and is equipped, right under the seal, with a plexiglass-covered inspection port through which oil splashing against the bottom of the scraper housing could be seen.

Clearances in the cross head and the bearings were such that the lateral motion of the rod was measured (statically, with an indicator) to be of an amplitude of 60 μm.

The rig was driven at 1800 RPM with a constant speed electric motor and operated without problems from the outset for about 400 hours. At that point a reddish oily substance appeared on top of the compliant housing. Inspection revealed that the substance was a mixture of oil and Rulon dust from the cap seal. In fact, it was found that the scraper area was choked with Rulon dust.

Upon further investigation it was found that the cap seal was wearing excessively since the roughness of the rod was seriously out of specification (4-5 micro inches compared to the specified 14-18 micro inches). Also the particular orientation of the rod seal with the scraper below the cap seal caused the wear particles to accumulate at the scraper area.

The scraper assembly was cleaned and reinstalled (with the same scraper)

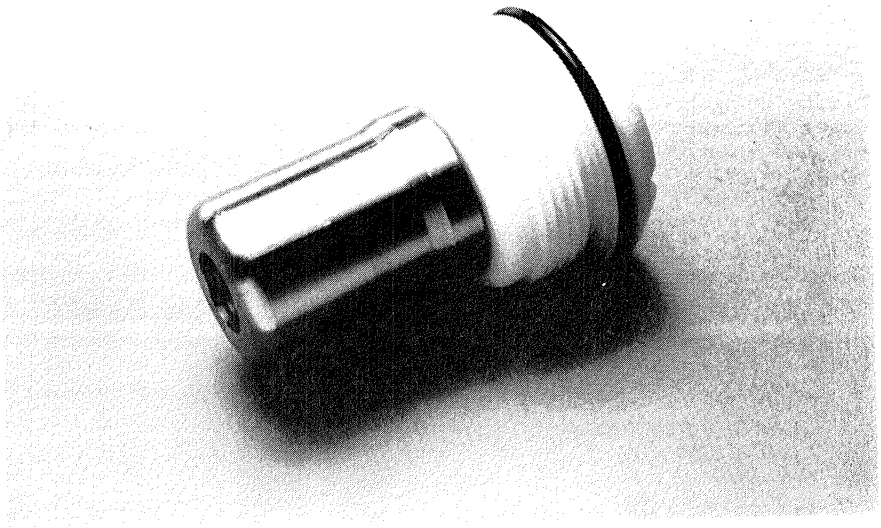

Figure 3.2

Scraper rod seal assembly

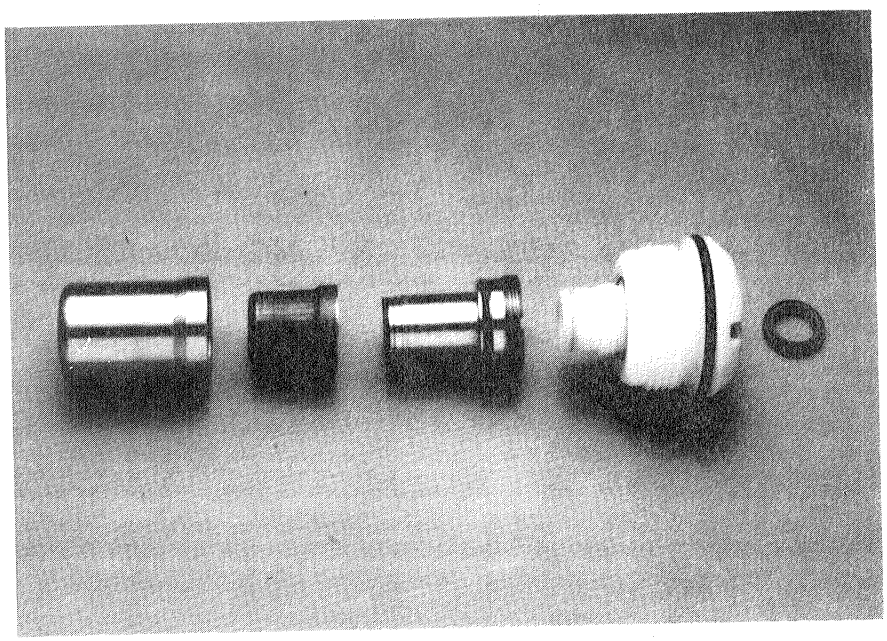

Figure 3.3

Scraper rod seal, partially disassembled. (From right: capseal, compliant housing, scraper body assembly, crown spring, scraper housing)

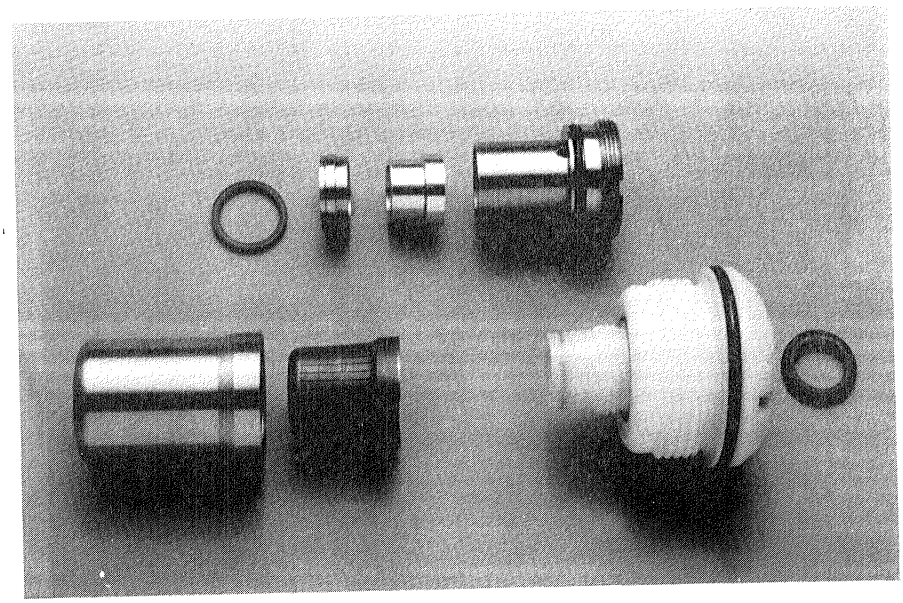

Figure 3.4

Scraper rod seal components (Top, from right: Scraper body, scraper, spacer, square rubber ring)

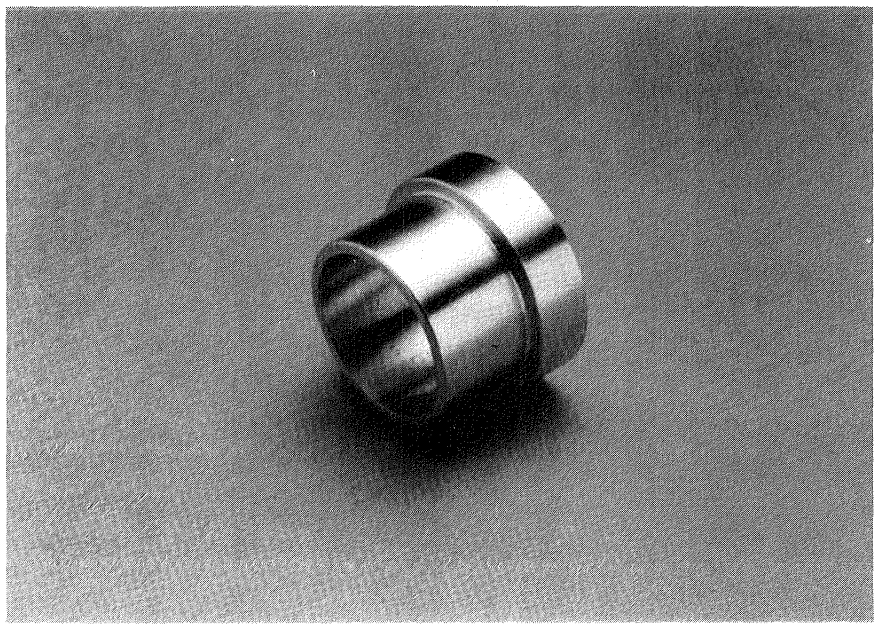

Figure 3.5
Scraper

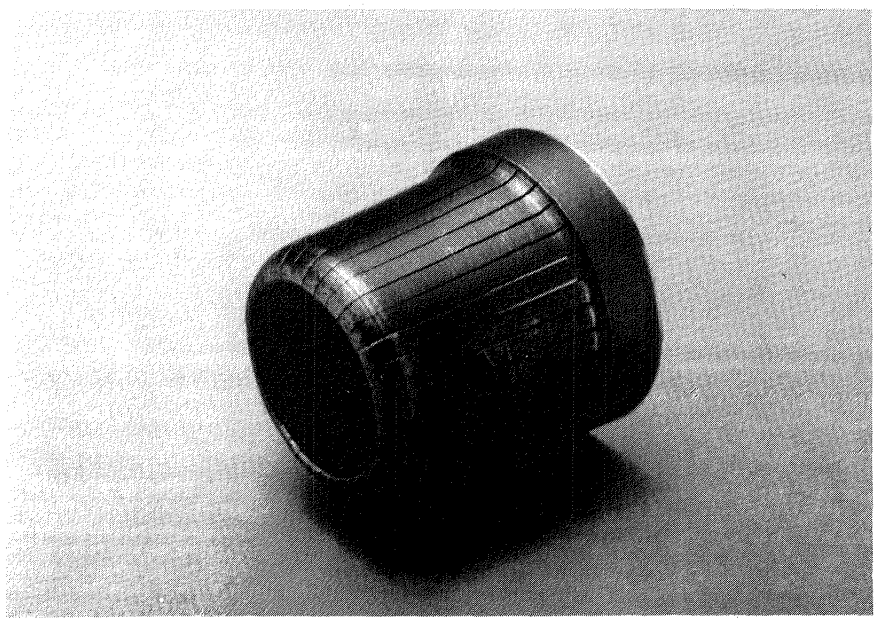

Figure 3.6
Crown Spring

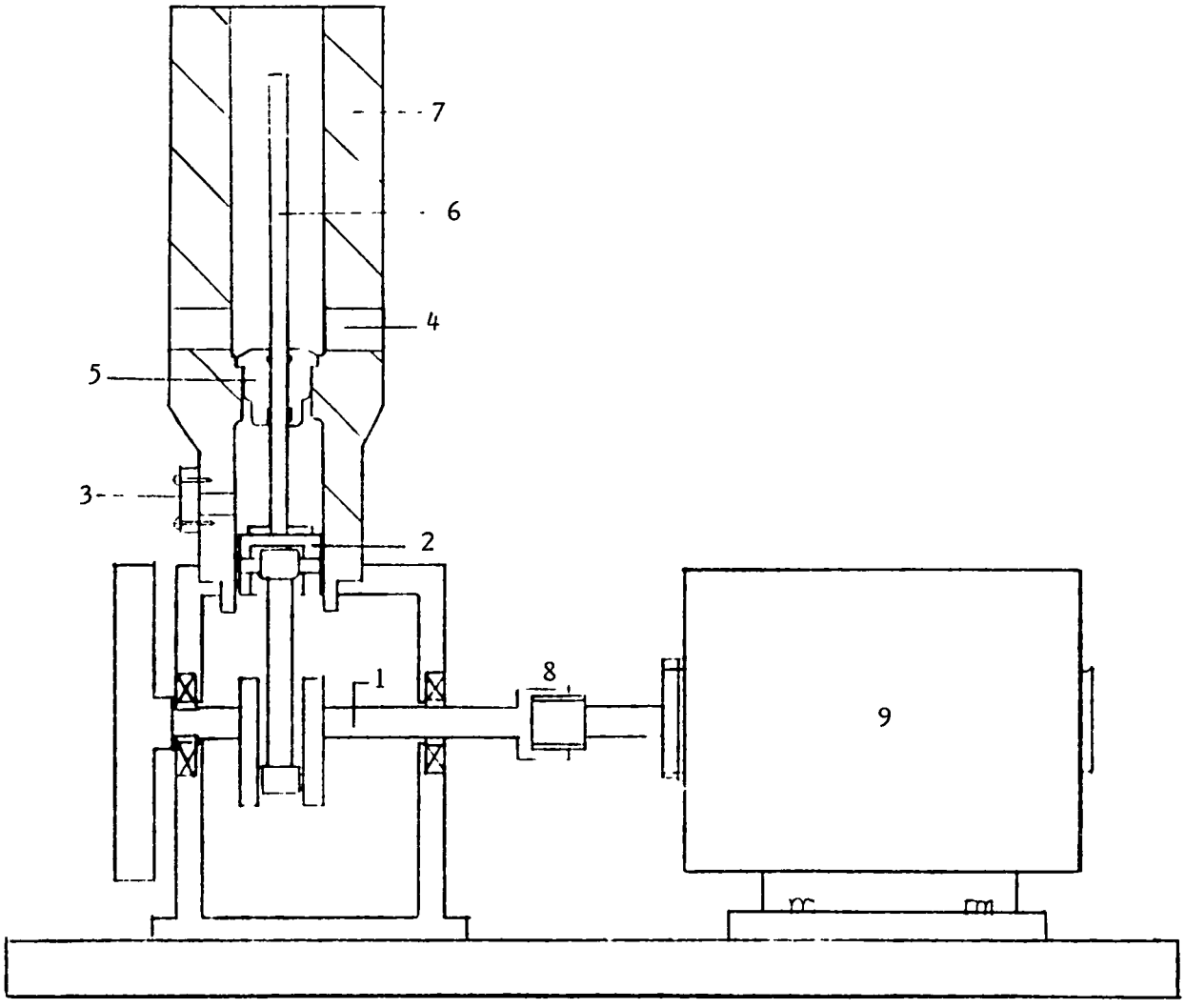

Figure 3.7

Rod Seal Endurance Test Rig, Schematic

(1) Crank shaft (2) Cross heads (3) Plexiglas covered inspection port
(5) Scraper rod seal (6) Piston rod (7) Cylinder (8) Coupling
(9) Constant speed AC motor

and was operating perfectly again, from the outset.

By July 8, the scraper had completed a total of 6750 running hours.

The endurance test strongly indicates that the scraper seal in its compliant housing will operate very well in an engine with a pressurized crankcase. It is recommended that this seal be tested further under more realistic conditions and that, perhaps, some quantitative data relative to friction, wear and oil permeation be taken.

Testing of the scraper assembly as a containment seal was performed on the variable speed rig described in Section 2.4 above. Indeed, it was the scraper assembly, acting as a containment seal, which allowed pressurization of the rig and performing the piston ring tests.

The first problem was the limited tensile strength of the compliant housing: it broke at mean pressure value of 8 MPa. This happened early in the program and for the balance thereof no attempt was made to go to mean pressure values higher than 5 MPa.

At pressures below 5 MPa the following trend was observed: starting at low pressure and increasing the pressure monotonically in steps, the seal performed rather well, containing the gas pressure and preventing oil migration. Upon reversing the process and going down with the pressure the seal continued to contain the gas pressure, but developed oil leakage.

Further investigation, by pressurizing the compliant housing in a fixture, revealed that under pressure the housing had undergone a skewed, off-axis deformation. It is hypothesized that such deformation, caused by slight deviation from axial symmetry, induced plastic deformation in the soft babbit scraper. Upon reducing the pressure, the geometry of the scraper no longer matched that of the rod and the scraper could no longer prevent oil migration.

Consequently, for the scraper assembly to function adequately with a

pressure difference across it the following should be done:

- The compliant housing should be redesigned using different materials and different geometry so that its compliance is retained and its tensile strength greatly increased.
- The scraper itself should be made of a different material with an elastic limit much greater than that of ASTM 3. Any such material is likely to be too hard and will not conform well at the contact area with the rod. Plating the scraper with a layer of soft metal will solve this problem.

SECTION 4 - HEAT PIPES

4.1 Introduction and Summary

The extensive use of heat pipes, indeed, their fundamental role in the Stirling engine concept of Stirling Thermal Motors, Inc., called attention to the fact that current high-temperature sodium heat pipe practice renders this simple device somewhat impractical.

The current practice calls for complex and expensive fabrication and handling procedures reflecting concerns that are, perhaps, justifiable in the nuclear power plant application (the major source of this technology) but seem undue in the Stirling engine application.

The purpose of the effort reported here was, generally, to demonstrate that sodium heat pipes for engine application are simple , practical devices.

In particular, the testing program was set to evaluate the following:

- Use of simple filling procedures involving commercial grade sodium, undistilled and handled in atmosphere
- Use of getters to avoid furnace degassing and increase the tolerance for air leakage
- Use of mechanical coupling to join heat pipe sections.

By July 8, 1985, a total of six heat pipes have accumulated about 46,000 operating hours. Six other heat pipes did not operate well at all. The unqualified success of the former and the failure of the latter clearly points at the following conclusions:

- Simple and crude filling procedures involving insertion of solid pieces of sodium, handled in air, into the open heat pipe prior to welding a cap and evacuating can be adequate. In addition, only

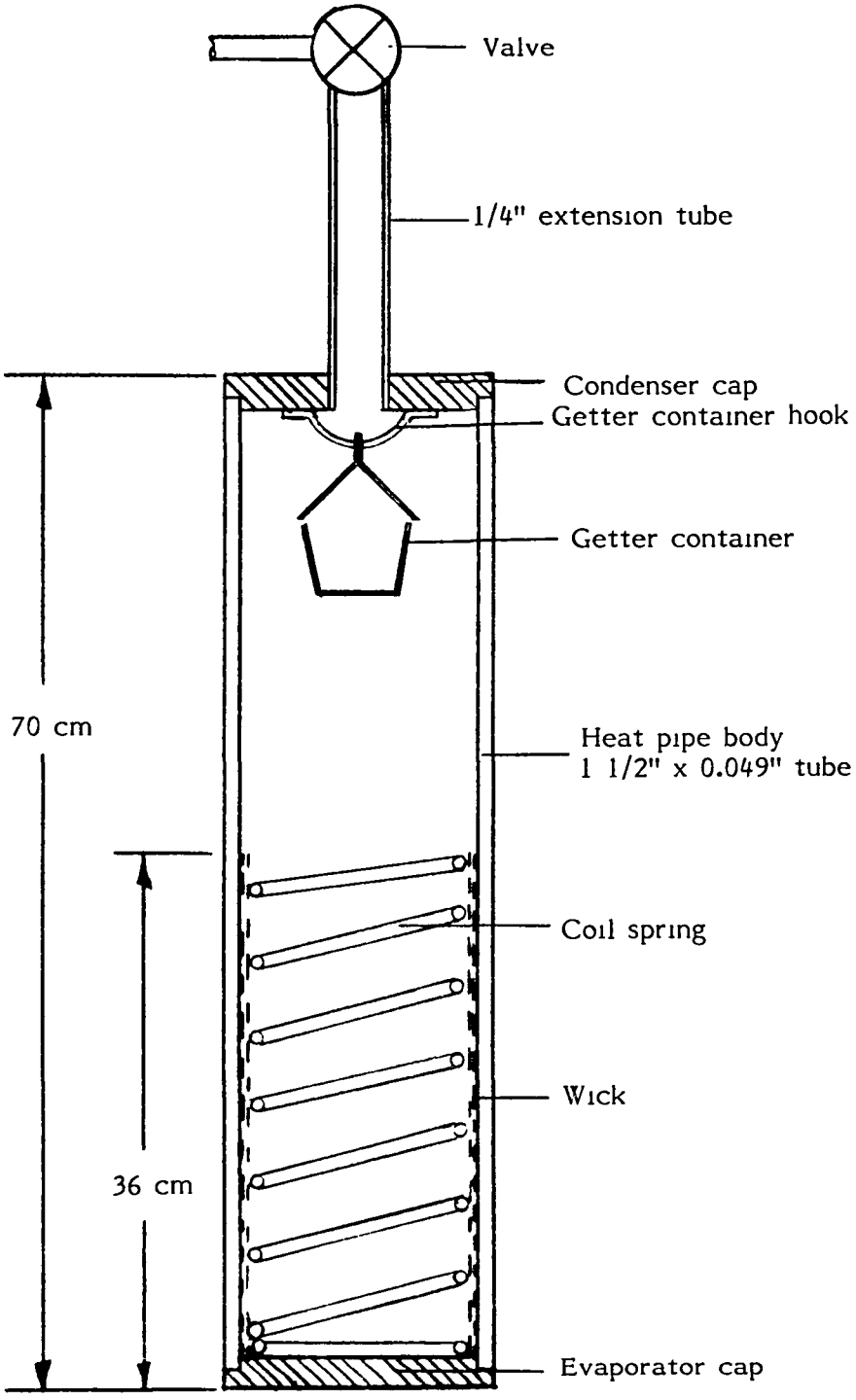

Figure 4.1

Typical Heat Pipe, Schematic

ready for normal operation.

Figure 4.2 shows, schematically, the various heat pipe configurations used. Table 4.1 summarizes some of their characteristics.

Heat pipes #2 and #3 are the base-line configuration and have no getters. Heat pipes #4 and #5 have getters contained in a perforated tube suspended in the condenser area from a hook attached to the condenser cap. This configuration proved unsuccessful since the calcium (which is one of the getters) melted at 830°C and leaked out through the holes in the getter tube, contaminating the wick. The temperature was, at the time, controlled manually at about 800°C, but, due to the difficulty of manual control, fluctuations occasionally brought the temperature above the melting point of the calcium. When the temperature would swing back the calcium would solidify in the wick and cause overheating of the contaminated region.

To address this problem heat pipes #6 and #8 were constructed with the getter contained in a "bucket" with a loosly fitted cover so that even if the calcium melted it would remain in the container and not contaminate the wick.

Heat pipes #7, #9, and #10 were built with a getter tube extending through the entire length of the heat pipe and with no valve. This was done in order to assess the possibility of avoiding the evacuation operation prior to start-up. The intention was to start the heat pipe up when full of atmospheric air and rely entirely on the getters to evacuate it by absorbing all the non-condensable gases. This concept did not prove successful and, due to lack of time, was not investigated further.

Heat pipes #11 and #12 were used to assess the feasibility of using the Conoseal couplings (available commercially from Aeroquip Corporation) shown in Figure 4.3. Since one of the requirements of the coupling is to provide capillary connection, these heat pipes were designed to operate against gravity,

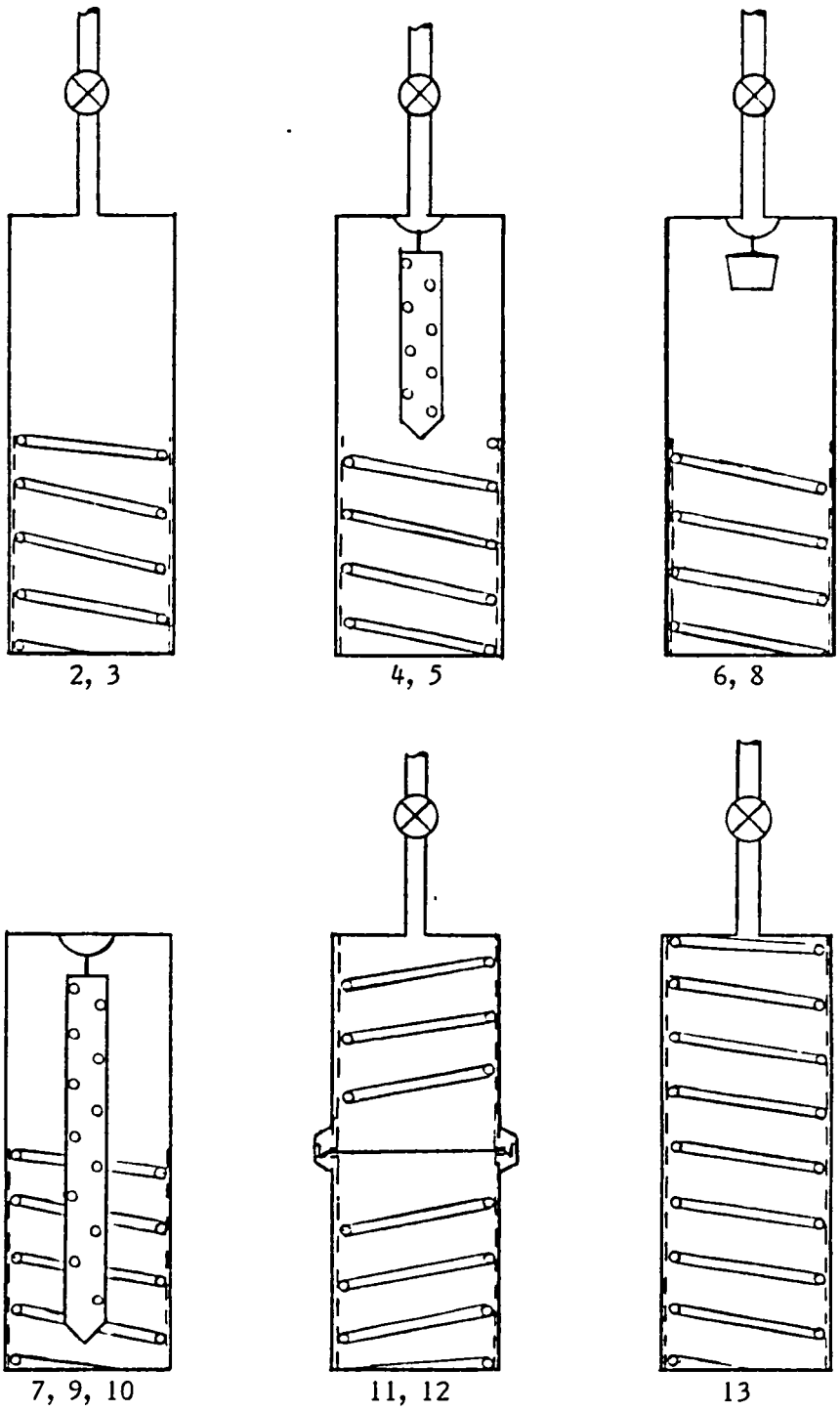

Figure 4.2

Configurations of the various heat pipes tested. Heat pipe numbers are indicated under the configuration schematics.

Table 4.1

Some Characteristics of Heat Pipes Tested

Heat Pipe #	Na	Ca	La	Zr	Spring	Mesh (316SS)
2	16	0	0	0	Ni-Cr	2 x 165 m, .002" w
3	16	0	0	0	Ni-Cr	2 x 165 m, .002" w
4	16	6	6	0	Ni-Cr	2 x 165 m, .002" w
5	16	6	6	0	Ni-Cr	2 x 165 m, .002" w
6	40	6.5	17.5	0	Ni-Cr	2 x 165 m, .002" w
7	40	13.5	19	0	Ni-Cr	2 x 165 m, .002" w
8	40	8	19	0	302SS	2 x 165 m, .002" w
9	40	14.5	14.5	5.2	302SS	2 x 165 m, .002" w
10	40	68	0	0	302SS	2 x 165 m, .002" w
11	40	0	0	9	302SS	3 x 165 m, .002" w
12	40	0	0	10	302SS	2 x 55 m, .004" w + 2 x 300 m, .0012"w
13	40	0	0	13	302SS	2 x 165 m, .002" w

Note: The weights of Na, Ca, La and Zr are in grams

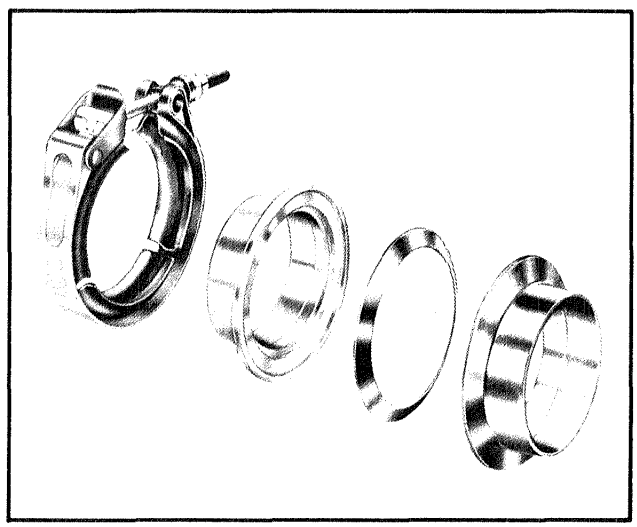

Figure 4.3

Medium Weight Conoseal Joint with T-bolt Quick Coupler

with the evaporator above the condenser, so that capillary pressure is relied upon to return the condensate to the evaporator. Consequently, the wick of heat pipes #11 and #12 extends into the condenser section as well. The capillary connection through the couplings is achieved as shown in Figure 4.4.

Heat pipe #13 is identical to #12 except that it has no coupling. It was intended to provide a comparison to the performance of heat pipe #12, but it failed quickly due to electric arcing in the tube furnace which was used to heat its evaporator.

Heat pipes #12 and #13 also contained some loose zirconium in the condensate path. The zirconium was intended to catalize the dissociation of corrosive Na O and bind the free oxygen. No analysis of heat pipe samples has been performed to confirm the effectiveness of the zirconium.

In summary, heat pipes #2, #3, #6, #8, #11, and #12 were useful configurations which were subjected to long term testing as described in the following Section 4.3.

4.3 Description of the Tests and Their Results

The heat pipe test stand is shown in Figure 4.5. Heat was provided to the evaporators by electric tube furnaces with maximum capacity of 1.5 kW. Two thermocouples were attached to the OD of each heat pipe, one in the evaporator and one in the condenser area. These were used to monitor and control the evaporator temperature, at first manually and later automatically, using temperature controllers, at 800°C.

Heat was dissipated from the condensers by radiation to the surroundings. The total heat transport was determined by the amount of insulation around the condensers. Most of the tests were performed at heat transport rate of about 0.75-1.0 kW.

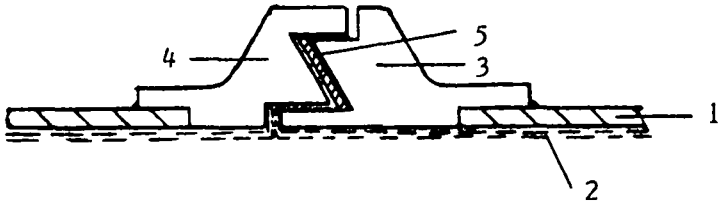

Figure 4.4

Capillary Connection through Conoseal Couplings

1) Heat pipe body
2) Wick
3) Male flange
4) Female flange
5) Sealing element

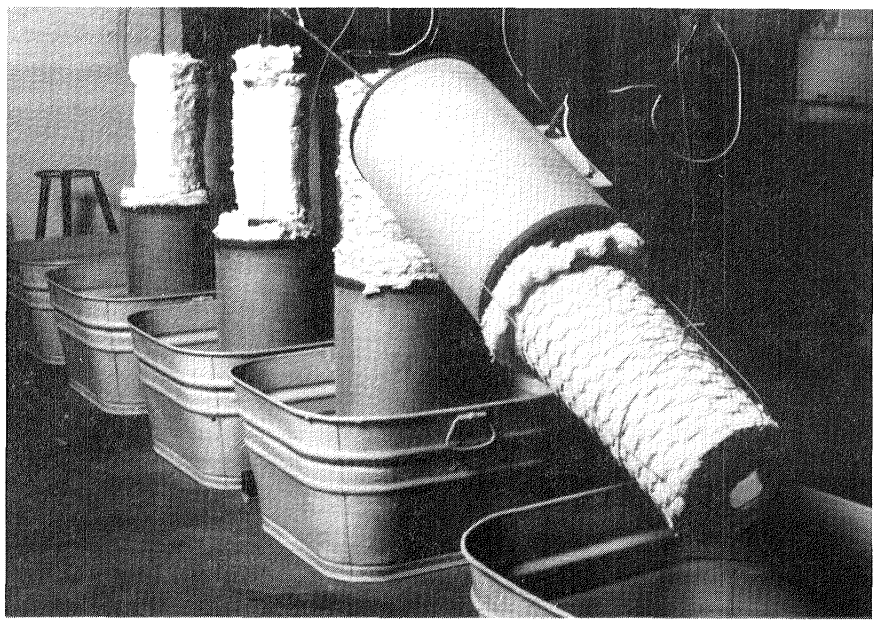

Figure 4.5

Heat Pipe Test Stand

(Shown, from right, Heat Pipes #12, #8, #11, #3)

Heat pipes #3 and #8, the former without getter and the latter with, have operated continuously from start-up and are still operating. On July 8, 1985, each of these heat pipes had completed 12,000 hours of problem-free operation. no difference between the two heat pipes was evident.

Heat pipes #2 and #6 operated with no problems until each accumulated 2000 hours. At that point, in order to assess the tolerance of the heat pipes to air leakage, metered doses of air were introduced into each heat pipe. Each dose was of 2.0 Ncc of air.

Heat pipe #6 (with getters) took about 15 minutes to recover from each dose of air, that is to absorb and bind 2.0 Ncc of air. Surprisingly, heat pipe #2 (without getter) also recovered and absorbed the air, but at a much slower rate, of about 15-20 hours per dose of 2.0 Ncc.

It appears that in the absense of getters the sodium itself acts as a getter forming oxides, nitrides and carbonates, and can handle leaks of up to 0.1 Ncc/hour until all the excess sodium inventory is consumed.

During the next 1000 hours of operation, dosing continued until a total of 58 doses (about 120 Ncc of air) were introduced into each heat pipe. At that point, with both heat pipes still operating perfectly, the test was stopped and heat pipe #2 was sent out for metalographic inspection.

By July 8, 1985, heat pipe #2 had been inspected and found to be in rather good condition, with only slight evidence of corrosion and element transport. The metalographic inspection report is reproduced in Appendix III.

Heat pipes #11 and #12 are being tested in order to evaluate the Conoseal coupling. Heat pipe #11 is continuously cycled between 800°C and about 150°C, with each cycle taking 2 hours. Figure 4.6 shows a close-up of the coupling

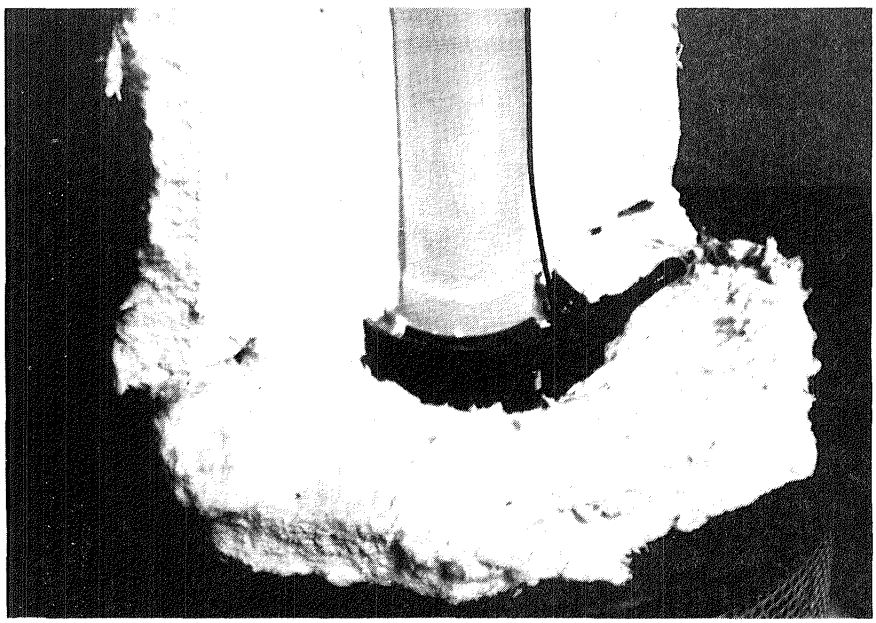

Figure 4.6

Conoseal Coupling in Operation

(Heat Pipe #11 at 800°C)

operating at 800°C. By July 8, 1985, heat pipe #11 had completed 4200 cycles and was still operating.

Heat pipe #12 was operated continuously against gravity to assess the capillary connection through the coupling. The maximum capillary pressure was determined experimentally to correspond to a maximum pumping height of 32 cm. The heat pipe was installed at an angle with the evaporator 32 cm above the condensor (right in Figure 4.5). Any degradation of the performance would immediately be detected by a general drop in temperature since the controlling thermocouple is at the highest point of the evaporator. By July 8, 1985, heat pipe #12 had completed 8000 hours of operation with no problems and no degradation of performance.

SECTION 5 - SPLIT SHAFT COMPONENT DESIGN

5.1 - Introduction and Summary

A swashplate drive for a Stirling engine is characterized by a heavy bending moment acting on the main shaft. As a result, the unsupported ends of the shaft tend to deflect appreciably.

In a swashplate engine with pressurized crankcase and a rotating shaft seal containing the crankcase pressure, the deflection of the shaft at the location of the rotating seal may be more than the amount that the seal can tolerate without affecting life and leakage rate. Therefore, a means is needed to eliminate shaft runout at the rotating seal.

The problem may be specifically illustrated by the original design of the STM4-120 variable swashplate Stirling engine of Stirling Thermal Motors, Inc., shown in Figure 5.1.

The main shaft (4) is supported by two closely spaced spherical roller bearings (6) and (9), to minimize deflection due to the bending moment applied by the swashplate (8), and a tapered roller bearing (2) to support the pressure induced thrust load and minimize shaft runout at the rotating seal (1). A substantial deflection slope at the rotating shaft seal (1) may adversely effect the life and performance of the seal.

A solution should be found without increasing the load (thus reducing the life) of the main bearings. In the specific case of the STM4-120 engine the problem is complicated by the fact that a narrow-clearance bushing (not shown) at the front end of the shaft is required for lubrication and hydraulic fluid management. These require that the runout at that end of the shaft is also low.

The proposed solution is the use of a split shaft design separating the shaft into two parts as shown in Figure 5.2. The first part (11) is the main

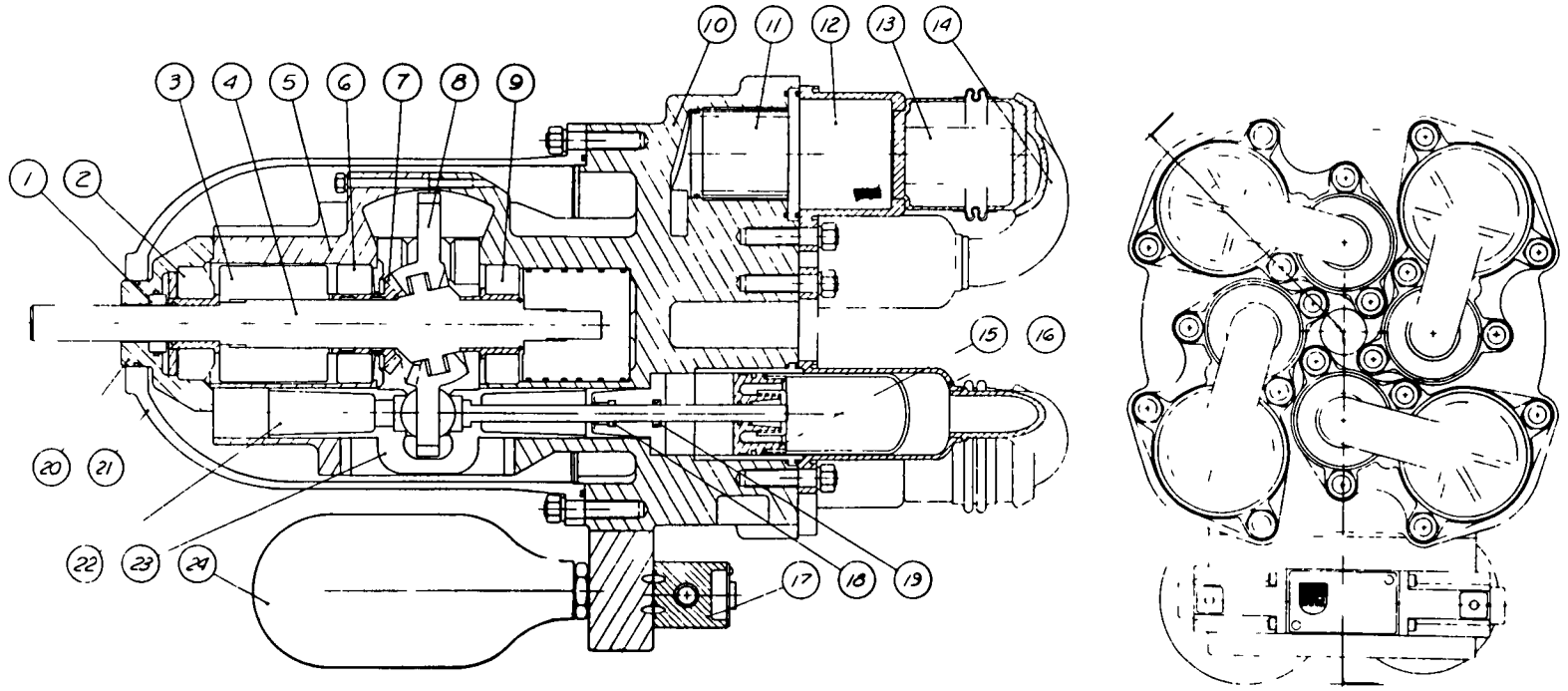

Figure 5.1

The STM4-120 Variable Swashplate Engine

1) Rotating shaft seal
2) Thrust bearing
3) Stroke converter
4) Main shaft
5) Rear crankcase casting
6) Rear main bearing
7) Bevel gear
8) Swashplate
9) Front main bearing
10) Front crankcase casting
11) Cooler
12) Regenerator
13) Heater
14) Hot connecting duct
15) Piston
16) Cylinder
17) Power control valve
18) Oil scraper
19) Cap seal
20) Rotating seal housing
21) Pressure hull
22) Cross-head
23) Cross head bridge
24) Hydraulic accumulator

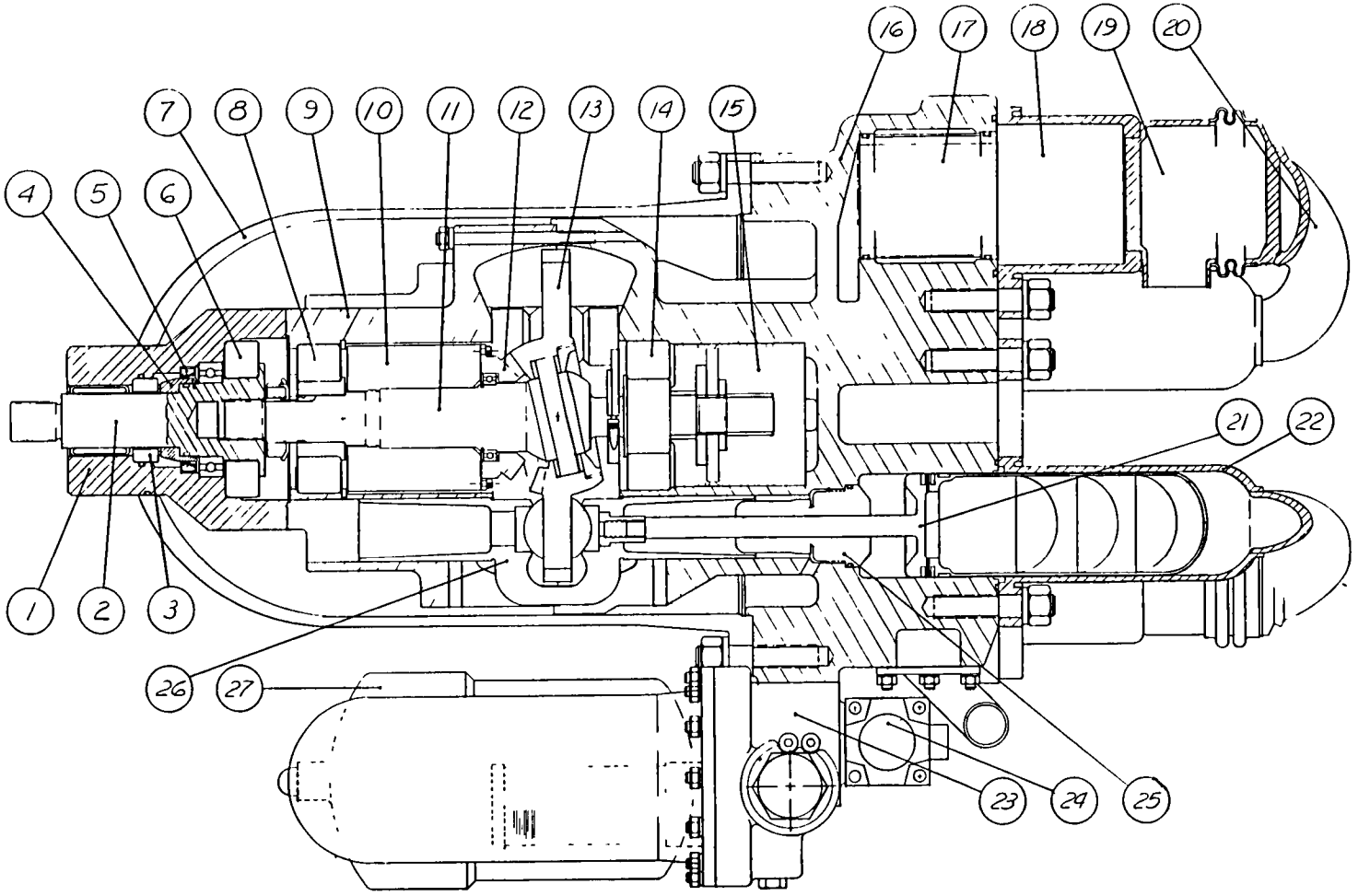

Figure 5.2
The STM4-120 Variable Swashplate Stirling Engine with a Split-shaft Design

1) Rotating shaft seal assembly
2) Drive shaft
3) Rotating shaft seal
4) Mating ring
5) Radial lip seal
6) Thrust bearing
7) Pressure hull
8) Rear main bearing
9) Rear crankcase
10) Rotary actuator
11) Main shaft
12) Bevel gear
13) Swashplate
14) Front main bearing
15) Oil pump module
16) Front crankcase
17) Cooler
18) Regenerator
19) Heater
20) Hot connecting duct
21) Piston assembly
22) Cylinder/regenerator housing
23) Hydraulic service assembly
24) Power control valve
25) Oil scraper/capseal ass'y
26) Crosshead
27) Accumulator

shaft to which the swashplate (13) is attached. This main shaft is supported by the main bearings (8) and (14) and is subjected to the bending moment. The second part (2) is the drive shaft, subjected only to thrust load, which carries the seal (3) and its mating ring (4).

The main shaft (11) and the drive shaft (2) are splined together. The spline permits the main shaft to deflect freely without transmitting transverse load or moment to the drive shaft. The latter runs true with no deflection at the seal. The spline clearance accomodates the slight misalignment due to the deflection of the main shaft.

In addition, judicious selection of the cross-sectional dimensions of the various sections of the main shaft greatly reduces its deflection at the front end where the bushings of the oil pump module (15) are located.

Under this program a variable swashplate drive design was completed which incorporates the split shaft and a separate end seal assembly. The design was based on a reference variable swashplate design (STM4-120) previously generated by Stirling Thermal Motors, Inc.

The design, set forth in the set of drawings attached to this report, achieved the following results:

(1) At the spline the main shaft deflection is 0.10 mm and the slope is 0.11 degrees. At the pump module end both deflection and slope of the main shaft vanish.

(2) The spline clearance was chosen to accomodate the 0.1 mm deflection and 0.11 degree slope of the main shaft. Compressive stress on the sides of the spline teeth determine its life to be more than 10,000 hours at full load.

(3) With the main shaft allowed to deflect freely, the calculated main bearing's life is 13,000 hours at full load.

The shaft deflection analysis, bearing life and spline strength calculations are presented in the following sections.

5.2 - Main Shaft Deflection Analysis

It may be recalled that one of the design requirements is that the deflection and slope at the front end of the shaft vanish. The energy method is used to evaluate the cross sectional dimension of the main shaft which satisfies this requirement. A free body diagram of the main shaft and its model is shown in Figure 5.3. The main shaft has five different sections as shown in the figure. Section #4 was chosen for adjusting the deflection slope at the front main bearing since it is the closest to that bearing, has the highest influence, and is relatively free from other design constraints.

The main bearings are treated as simple supports where the deflection vanishes and hence vanishing slope at the front main bearing means vanishing deflection and slope in the entire region to its right.

Coordinates and dimensions are defined in Figure 5.3. Table 5.1 presents the positions, cross sectional dimensions, and sectional moments of inertia of the various shaft model sections.

A virtual moment (m) is applied at the front main bearing. The deflection slope at that point (θ) is determined by differentiation of the elastic strain energy with respect to the virtual moment and evaluating the derivative for a vanishing virtual moment ($m = 0$). Demanding the slope to vanish yields one equation for the unknown moment of inertia of Section 4 (I_4) of the main shaft.

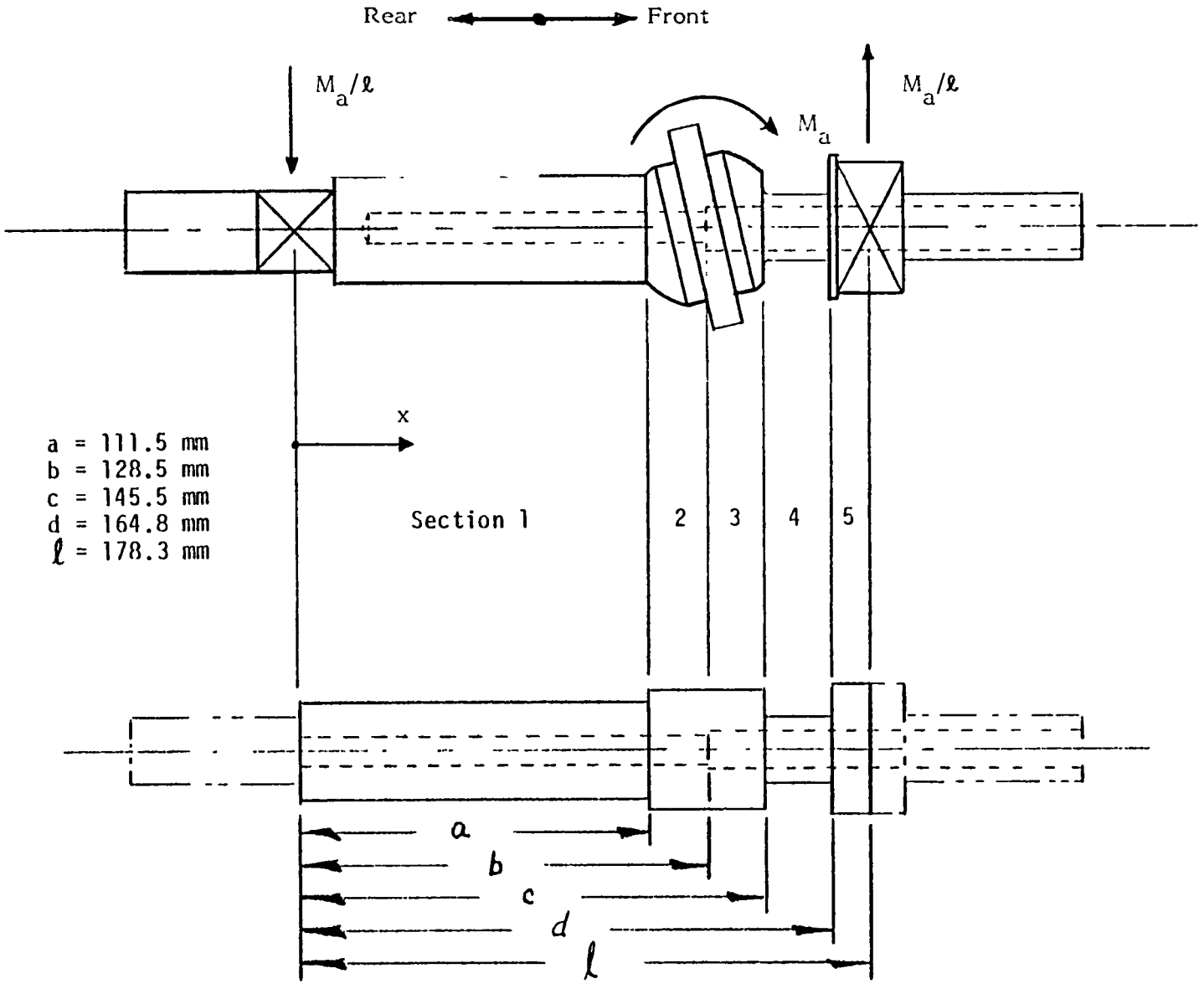

Figure 5.3

Free Body Diagram of Main Shaft

Shaft model is shown underneath. Main bearings are considered simple supports.

Table 5.1

Shaft Model Cross Sectional Dimensions

Section	Position (mm)	OD(mm)	ID(mm)	Moment of Inertia(mm^4)
1	$0 \leq x \leq 111.5$	32.0	11.0	5.075×10^4
2	$111.5 \leq x \leq 128.5$	38.0	11.0	1.016×10^5
3	$128.5 \leq x \leq 145.5$	38.0	14.0	1.005×10^5
4	$145.5 \leq x \leq 164.8$	TBD	14.0	TBD
5	$164.8 \leq x \leq 178.3$	40.0	14.0	1.238×10^5

The moment function is:

$$M(x) = \begin{cases} (M_a + m)\ x/\ell & @ \quad 0 \le x \le b \\ (M_a + m)\ x/\ell - M_a & @ \quad b \le x \le \ell \end{cases} \tag{5.1}$$

The strain energy:

$$U = \int_o^{\ell} \frac{1}{2} \frac{M^2(x)}{EI}\, dx \tag{5.2}$$

The deflection slope at the front main bearing:

$$\theta = \left.\frac{\partial U}{\partial m}\right|_{m=0} = \left[\int_o^{\ell} \frac{M(x)}{EI} \left(\frac{\partial M(x)}{\partial m}\right) dx\right]_{m=0} \tag{5.3}$$

Substitution of 5.1 in 5.3, carrying out the differentiations, taking into account the different sectional moments of inertia and setting $\theta = 0$ yield the equations for I_4:

$$\frac{M_a}{E}\left\{\frac{1}{I_1}\int_o^a \left(\frac{x}{\ell}\right)^2 dx + \frac{1}{I_2}\int_a^b \left(\frac{x}{\ell}\right)^2 dx + \frac{1}{I_3}\int_b^c \frac{x}{\ell}\left(\frac{x}{\ell} - 1\right) dx + \right.$$

$$\left. + \frac{1}{I_u}\int_c^d \frac{x}{\ell}\left(\frac{x}{\ell} - 1\right) dx + \frac{1}{I_5}\int_d^{\ell} \frac{x}{\ell}\left(\frac{x}{\ell} - 1\right) dx\right\} = 0 \tag{5.4}$$

The expression in the brackets can be made to vanish independently of the magnitude of the applied moment and the shaft material. Substitution of the values for I_1, I_2, I_3 and I_5 from Table 5.1 and solving 5.4 for I_4 yields:

$$I = 6580 \text{ mm}$$

With an ID of 14 mm, this corresponds to an OD of 20.4 mm for section 4.

With the shaft geometry thus fully determined the moment function is integrated twice to yield the deflection slope and the deflection.

The integration is carried out with the following quantities:

Applied moment M_a = 1100 N.m (corresponding to full load)

Elastic modulus E = 2.0 x 10 (AISI 8620)

The two required integration constants are supplied by the two boundary conditions which require that the deflection at the two main bearings vanish.

The results are shown in Figure 5.4 and tabulated in Table 5.2.

5.3 - Bearing Life Calculations

The functions of the main shaft bearings in the STM4-120 are to provide radial support for the main shaft while allowing angular deflections (slope) at the bearing, and to provide axial location of the shaft. The latter function requires a bearing with some thrust capacity to prevent axial displacements of the shaft. Spherical roller bearings are an ideal choice for this application since they have high radial load capacity, some thrust load capacity, and allow small angular deflections without adversely affecting performance.

The main shaft bearings specified are SKF 22208C spherical roller bearings with a Basic Dynamic Capacity (C_{10}) of 63,600 N.

From the free-body diagram below, the bearing reactions are,

$$R_1 = - R_2 = M_a/\ell$$

The maximum value of the applied moment in the STM4-120 engine is M = 1100 Nm, and the bearing span, ℓ = 178 mm, yielding bearing reactions $R_1 = -R_2 = 6180N$.

The L_{10} life, in hours, for roller bearings is:

$$L_{10} = \frac{16667}{N} \left(\frac{C_{10}}{P}\right)^{10/3}$$

78

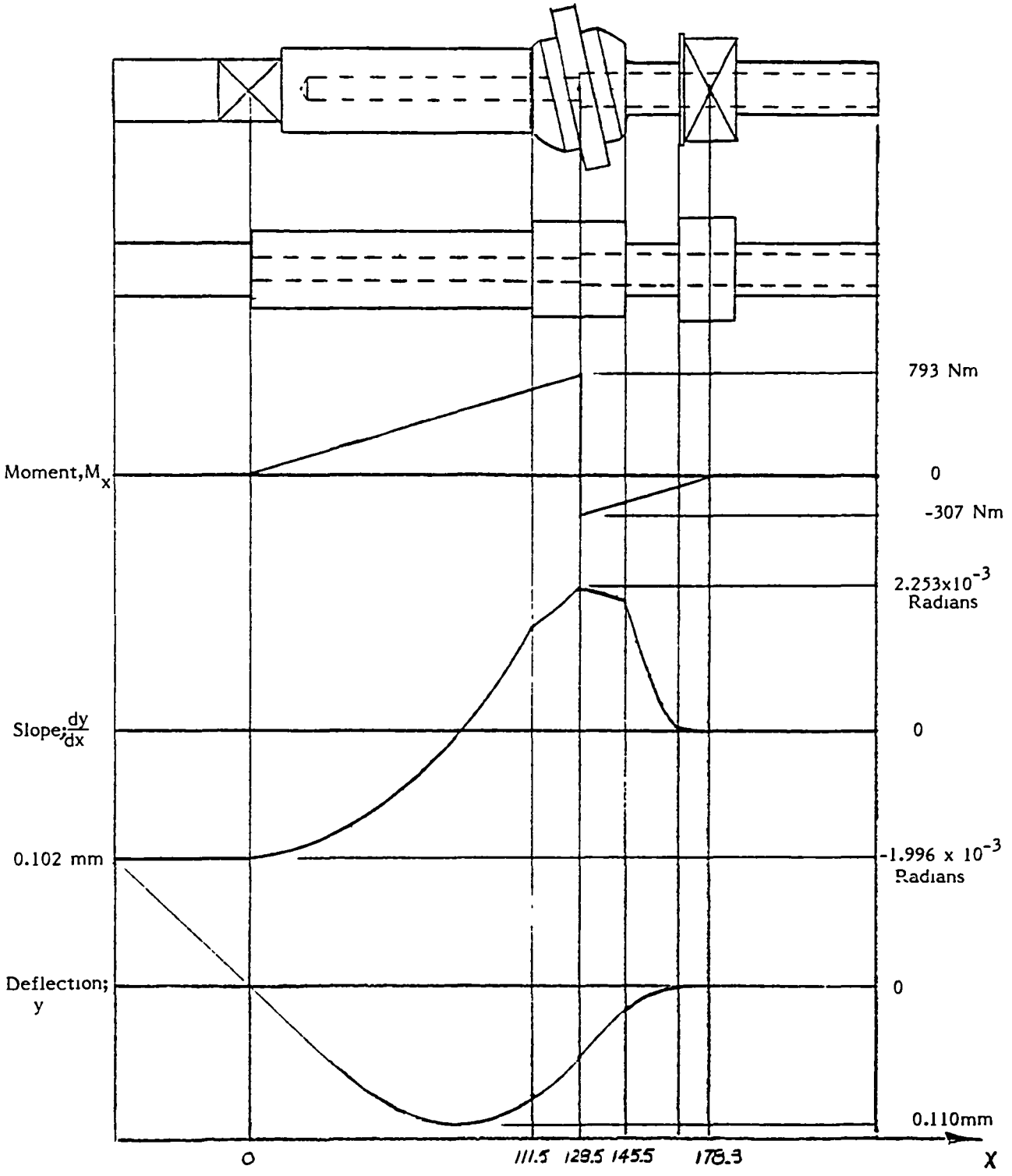

Figure 5.4

Main Shaft Moment, Slope and Deflection at Full Load

Table 5.2

Main Shaft Deflection (y) and Slope (dy/dx) at Various Positions (x) Along the Axis at Full Load

x	y	$\frac{dy}{dx}$	
(mm)	(mm)	(RAD)	(DEG)
0	0	-1.996×10^{-3}	-0.1144
10	-0.0199	-1.967×10^{-3}	-0.0027
30	-0.0391	-1.879	-0.1076
40	-0.0736	-1.732	-0.0992
50	-0.0875	-1.262	-0.0723
60	-0.0989	-0.939	-0.0538
70	-0.1061	-0.557	-0.0319
75	-0.1084	-0.344	-0.0197
82.45	-0.1097	0	0
90	-0.1082	+0.382	+0.0219
100	-0.1017	+0.940	+0.0539
111.5	-0.0868	+1.655	+0.0948
115	-0.0808	+1.771	+0.1015
120	-0.0715	+1.943	+0.1113
125	-0.0614	+2.123	+0.1216
128.5	-0.0537	+2.253	+0.1291
130	-0.0504	+2.232	+0.1279
135	-0.0394	+2.164	+0.1240
140	-0.0287	+2.104	+0.1205
145.5	-0.0173	+2.046	+0.1172
150	-0.0096	+1.423	+0.0815
155	-0.0040	+0.839	+0.0480
160	-0.0010	+0.367	+0.0211
164.8	-0.0001	+0.022	+0.0012
170	-0.0000	+0.008	+0.0005
175	-0.0000	+0.001	+0.0001
178.3	0	0	0

where

N = speed in RPM

C_{10} = Basic Dynamic Capacity

P = maximum radial load

The maximum speed of the STM4-120 is 300 RPM, therefore, the L_{10} life of the main bearings is:

$$L_{10} = \frac{16667}{3000} \left(\frac{63600\ N}{6180\ N}\right)^{10/3} = 13200 \text{ hours}$$

The drive shaft in the STM4-120 transmits the shaft torque through the wall of the pressurized crankcase. The crankcase pressure, contained by a mechanical face seal, exerts a thrust force on the drive shaft equal to the crankcase pressure times the seal area.

The specified thrust bearing is a Timken TTHD-T1750 tapered roller bearing with a Basic Dynamic Thrust Rating (C_{90}) of 32,200N at 500 RPM.

The thrust load, T_e, due to the crankcase pressure, is:

$$T_e = p_m A_s = p_m \left(\frac{\pi}{4} d_s^2\right)$$

where

p_m = crankcase mean pressure = 11 MPa

A_s = seal area

d_s = seal diameter = 37 mm

Therefore, the thrust load is

$$T_e = (11 \text{ MPa}) \left(\frac{\pi}{4}\right) (37 \text{ mm})^2 = 11{,}830N$$

The L_{10} life of tapered roller bearings can be calculated from the following equation from the Timken Engineering Journal

$$L_{10} = \left(\frac{C_{90} \times SF}{T_e}\right)^{10/3} (3000 \text{ hrs})$$

where

C_{90} = Basic Dynamic Load Rating

SF = speed factor = $\left(\frac{500}{rpm}\right)^{3/10} = \left(\frac{500}{3000}\right)^{3/10} = 0.584$

T_e = Load

Substituting the appropriate values in this equation yields an L_{10} life of:

$$L_{10} \left(\frac{32200 \times .584}{11830}\right)^{10/3} (3000) = 14{,}060 \text{ hrs.}$$

5.4 - Spline Strength Calculations

The torque capacity of involute splines can be calculated using standard formulas and application factors, as in Machinery's Handbook, 22nd Edition, pp 922-927. The torque capacity of a spline is determined by evaluating its strength with regard to three types of spline failure; shear failure under the roots of external teeth and/or at the pitch diameter of the teeth, compressive failure at the faces of the teeth, and burst failure of the internal spline. Internal splines may burst due to three kinds of tensile stress; (1) tensile stress due to the radial component of the transmitted load; (2) centrifugal tensile stress; and (3) tensile stress due to the tangential force at the pitch

line causing bending of the teeth.

The spline chosen to mate the main shaft with the drive shaft has 30 teeth, a 0.75 module and a 30° pressure angle. The tolerance class was chosen to allow sufficient clearance to accomodate the deflection of the main shaft. The spline is designated as follows:

INT/EXT 30Z x 0.75 m x 30.0 R x 5H/5d

ANSI B92.2M - 1980

The stresses in the designated spline are calculated below.

Shear Stress Under the Roots of External Teeth:

For a transmitted torque T, the torsional shear stress (τ_1) induced in the shaft under the root diameter of an external spline is:

$$\tau_1 = \frac{16\ T\ Ka}{D_{re}{}^3 K_f} = \frac{16 \times 1.25 \times 10^5 \text{N mm} \times 1.0}{\times (20.81\ \text{mm})^3 \times 1.0} = 71\ \text{MPa}$$

where

T = transmitted torque = 125 Nm

D_{re} = minor diameter = 20.81 mm

K_a = spline application factor for a uniform power source and uniform load = 1.0

K_f = spline fatigue life factor for 10,000 torque cycles = 1.0. (a torque cycle consists of one start and one stop, not the number of revolutions.)

Since the maximum allowable shear stress for case hardened steel (58-63 Rc) as specified for the STM4-120 is 345 MPa, the spline strength with regard

to shear stress under roots of the external teeth is more than sufficient.

Shear Stress at the Pitch Diameter of Teeth:

The shear stress at the pitch line of the teeth for a transmitted torque, T is:

$$\tau_2 = \frac{4\,T\,K_m\,K_a}{D\,N\,L_e\,t\,K_f} \qquad \frac{4 \times 1.2 \times 10^5 \text{N mm} \times 1.0 \times 1.0}{22.5 \text{ mm} \times 30 \times 22.5 \text{ mm} \times 1{,}062 \text{ mm} \times 1.0} = 31 \text{ MPa}$$

where

T = transmitted torque

K_a = spline application factor

K_m = load distribution factor for misalignment of flexible splines for misalignment of .002 m/mm and 22.5 mm face width = 1.0

D = pitch diameter = 22.5 mm

N = number of teeth = 30

L_e = spline effective length = full length of spline for pitch diameters less than 25 mm = 22.5 mm

t = actual circular tooth thickness = 1.062 mm

K_f = spline fatigue life factor

Again, the induced stress of 31 MPa is much lower than the maximum allowable stress of 345 MPa, hence the spline strength is more than sufficient with regard to shear stress at the pitch diameter.

Compressive Stress on the Sides of the Spline Teeth:

Allowable compressive stresses on splines are very much lower than for gear teeth since non-uniform load distribution and misalignment result in unequal load sharing and end loading at the teeth.

For a transmitted torque, T, the compressive stress on the sides of the spline teeth is:

$$\sigma_c = \frac{2\,T\,K_m\,K_a}{D\,N\,L_e\,m\,K_w} = \frac{2 \times 1.25 \times 10^5\ \text{N mm} \times 1.0 \times 1.0}{22.5\ \text{mm} \times 30 \times 22.5\ \text{mm} \times 0.75 \times 0.7} = 31.3\ \text{MPa}$$

where

m = spline module = 0.75 (the module is the inverse of the diametral pitch)

K_w = wear life factor for flexible splines = 0.7 for 10,000 hours at 3000 RPM (1×10^9 revolutions)

Here the maximum compressive stress is less than the allowable compressive stress of 35 MPa, indicating adequate performance for the design life of the spline.

Bursting Stress on the Internal Spline:

For a transmitted torque, T, the radial load tensile stress is:

$$\sigma_1 = \frac{T \tan\varphi}{\pi D\,t_w\,L} = \frac{1.25 \times 10^5\ \text{N mm} \times \tan 30.0^\circ}{\pi \times 22.5\ \text{mm} \times 9.0\ \text{mm} \times 22.5\ \text{mm}} = 5\ \text{MPa}$$

where

φ = pressure angle 30.0

t_w = wall thickness of internal spline = 1/2 (shaft OD - major dia.) = 9 mm

L = full length of spline = 22.5 mm

the centrifugal tensile stress is

$$\sigma_2 = 1.656 \times 10^{-6} \times (RPM)^2 \times (D_{oi}^2 + 0.212\ D_{ri}^2)$$

where

D_{oi} = OD of spline sleeve in inches = 1.563

D_{ri} = major diameter of internal spline in inches = $\frac{23.7}{25.4}$ = 1.563

$$\sigma_2 = 1.656 \times 10^{-6} \times 3000^2 \text{rpm} \times (1.563^2 + 0.212 \times 0.934^2) = 39 \text{ psi} = 0.3 \text{ MPa}$$

and the beam loading tensile stress is

$$\sigma_3 = \frac{4T}{D^2 L_e Y} = \frac{4 \times 1.25 \times 10^5 \text{ N mm}}{(22.5 \text{ mm})^2 \times 22.5 \text{ mm} \times 1.5} = 30 \text{ MPa}$$

where Y = Lewis form factor = 1.5 (for 30.0 pressure angle)

Total tensile stress tending to burst the rim of the external member:

$$\sigma_t = \frac{K_a K_m}{K_f} [(\sigma_1 + \sigma_3) + \sigma_2] = \frac{1.0 \times 1.0}{1.0} [(5 + 30) + 0.3] = 35.3 \text{ MPa}$$

The total tensile stress of 35 MPa is much lower than the allowable tensile stress of 380 MPa, indicating sufficient spline strength with regard to bursting.

APPENDIX I

PISTON RING LEAKAGE EFFECTS

Consider the upper piston ring of the set of 2 pumping piston rings shown in Figure 2.1.

The upper axial face of that ring is exposed to a harmonically variable pressure (p_u) with a mean value (p_m) and an amplitude (Δp).

The lower face of the ring is exposed to a constant pressure equal to the maximum variable pressure:

$$p_u = p_m + \Delta p \cos \omega t \tag{I.1}$$

$$p_\ell = p_m + \Delta p \tag{I.2}$$

where ω is the angular speed of the rig and t is time.

For laminar flow, leakage across the ring (defined as positive from the lower face to the upper face) is proportional to the pressure difference ($p_e - p_u$) and inversely proportional to the laminar resistance (R). The leakage mass flow rate ($\dot{m}$) is thus given by:

$$\dot{m} = \frac{1}{R} (p_\ell - p_u) = \frac{\Delta p}{R} (1 - \cos \omega t) \tag{I.3}$$

The leakage adds gas mass to the variable volume above the piston. That added mass at any point (Δm) is found by time integration of the mass flow rate ($\dot{m}$) given by Equation I.3.

$$\Delta m = \int \dot{m} \, dt = \frac{\Delta p}{\omega R} (\omega t - \sin \omega t + \varphi) \tag{I.4}$$

where φ is an (yet undetermined) integration constant.

The mass increase (Δm) raises the pressure p_u so that the disturbed pressure (p_u') in the volume above the ring is:

$$p_u' = p_u \left(1 + \frac{\Delta m}{m_o}\right) \tag{I.5}$$

where m is the undisturbed total gas mass in that volume.

Substitution of (I.1) and (I.4) in (I.5) yields:

$$p_u' = (p_m + \Delta p \cos \omega t) \left[1 + \frac{\Delta p}{m_o \omega R} (\omega t - \sin \omega t + \varphi)\right] \tag{I.6}$$

Since $\frac{\Delta p}{p_m}$ and $\frac{\Delta p}{m_o}$ are small quantities higher order terms in these quantities may be neglected with the following result:

$$p_u' \cong p_m + \Delta p \left[\cos \omega t + \frac{p_m}{m_o \omega R} (\omega t - \sin \omega t + \varphi)\right] \tag{I.7}$$

The ring is constructed so that when p_u' is larger than p_e the ring stops to seal and the extra mass in the variable volume will revert to the space below the ring. This happens just when $\omega t = 0$ and hence:

$$\begin{aligned} \Delta m &= 0 \quad @ \quad \omega t = 0 \quad (a) \\ p_u' &= p_m + \Delta p \quad @ \quad \omega t = 0 \quad (b) \end{aligned} \tag{I.8}$$

Application of (I.8) to (I.7) or to (I.4) determines the integration constant:

$$\varphi = 0 \tag{I.9}$$

and the disturbed pressure:

$$p_u' = p_m + \Delta p \left[\cos \omega t + \frac{p_m}{m_o \omega R} (\omega t - \sin \omega t)\right] \tag{I.10}$$

The pressure variation in the volume above the ring is caused by polytropic compression. The volume (V) varies harmonically with a mean value (Vm) and an amplitude (ΔV) due to the motion of the piston:

$$V = V_m - \Delta V \cos \omega t \tag{I.11}$$

The polytropic process enforces the following relation between the volume (V) and the pressure (p_u):

$$p_u V^n = p_m V_m^n \tag{I.12}$$

where n is the polytropic constant. Substitution of (I.1) and (I.11) in (I.12) yields:

$$1 + \frac{\Delta p}{p_m} \cos \omega t = (1 - \frac{\Delta V}{V_m} \cos \omega t)^{-n} \tag{I.13}$$

Since $\frac{\Delta V}{Vm}$ is a small quantity the right hand side of (I.13) may be expanded in a series with only thie first order term retained:

$$1 + \frac{\Delta p}{p_m} \cos \omega t \cong 1 + n \frac{\Delta V}{V_m} \cos \omega t \tag{I.14}$$

and thus:

$$\frac{\Delta p}{p_m} = n \frac{\Delta V}{V_m} \tag{I.15}$$

The work (W_{Lp}) performed (per cycle) by the gas undergoing the polytropic compression distrubed by leakage is given by integration over the cycle of:

$$dW_{Lp} = p'_u \frac{dV}{d(\omega t)} d(\omega t) \tag{I.16}$$

Conveniently defining $\alpha \equiv \omega t$ and integration (I.16):

$$W_{Lp} = \int_0^{2\pi} \left\{ p_m + \Delta p \left[\cos\alpha + \frac{p_m}{m_o \omega R} (\alpha - \sin\alpha) \right] \right\} \Delta V \sin\alpha \, d\alpha = -3\pi \Delta p \, \Delta V \frac{p_m}{m_o \omega R} \qquad (I.17)$$

The equation of state for the (ideal) gas requires that:

$$\frac{p_m}{m_o} = (C_p - C_v) \frac{T_m}{V_m} \qquad (I.18)$$

where c_p and c_v are the specific heat values of the gas at constant pressure and volume respectively and T_m is the mean volume temperature. Defining $\gamma \equiv c_p/c_v$ and substituting (I.15) in (I.17):

$$W_{Lp} = -3\pi \frac{p_m}{\omega R} n \frac{\gamma - 1}{\gamma} C_p T_m \left(\frac{\Delta V}{V_m}\right)^2 \qquad (I.19)$$

The same consideration applies to the lower ring of the pumping ring set and the variable volume below it so that the total work performed by the working gas in the rig due to this leakage effect is $2W_{Lp}$.

The total heat (Q_{Lp}) dissipated by the rig (per cycle) is found by applying the energy equation (for a cyclic process).

$$Q_{Lp} + 2 W_{Lp} = 0 \qquad (I.20)$$

which yields:

$$Q_{Lp} = 6\pi \frac{p_m}{\omega R} n \frac{\gamma - 1}{\gamma} C_p T_m \left(\frac{\Delta V}{V_m}\right)^2 \qquad (I.21)$$

An additional loss associated with the piston ring is the viscous dissipation in the leakage path. The volumetric flow ($\dot{\phi}$) undergoes a pressure drop ($p_\ell - p_u$) and thus

dissipates energy (W_{Lo}) as follows:

$$dW_{Lo} = \dot{\varphi} (p_{\ell} - p_u) dt = \frac{\dot{\varphi}}{\omega} \Delta p (1 - \cos\alpha) d\alpha \qquad (I.22)$$

The volumetric flow is:

$$\dot{\varphi} = \frac{\dot{m}}{\rho_m} \qquad (I.23)$$

where ρ_m is the mean gas density which, according to the equation of state is:

$$\rho_m = \frac{\gamma}{\gamma - 1} \frac{p_m}{C_p T_m} \qquad (I.24)$$

Thus:

$$dW_{Lo} = \frac{\gamma - 1}{\gamma} \frac{\dot{m}}{\omega} C_p T_m \frac{\Delta p}{p_m} (1 - \cos\alpha) d\alpha \qquad (I.25)$$

Substitution of (I.3) and (I.15) in (I.25) and integration over the cycle yields:

$$W_{Lo} = \frac{p_m}{\omega R} n^2 \frac{\gamma - 1}{\gamma} C_p T_m \left(\frac{\Delta V}{V_m}\right)^2 \int_o^{2\pi} (1 - \cos\alpha)^2 d\alpha = 3\pi \frac{p_m}{\omega R} n^2 \frac{\gamma - 1}{\gamma} C_p T_m \left(\frac{\Delta V}{V_m}\right)^2 \qquad (I.26)$$

Doubling this amount to account for the other ring of the set yields the total heat (Q_{Lo}) dissipated (per cycle) in the rig due to the resistance of the flow path:

$$Q_{Lo} = 6\pi \frac{p_m}{\omega R} n^2 \frac{\gamma - 1}{\gamma} C_p T_m \left(\frac{\Delta V}{V_m}\right)^2 \qquad (I.27)$$

The total leakage loss (Q_L) per cycle is the sum of the above two

effects:

$$Q_L = Q_{Lp} + Q_{Lo} = 6\pi \frac{p_m}{\omega R} n (n+1) \frac{\gamma - 1}{\gamma} C_p T_m \left(\frac{\Delta V}{V_m}\right)^2 \qquad (I.28)$$

The "leakage coefficient" (C_L) defined in Section 2.7.2 above should be given by:

$$C_L = 6\pi \frac{p_m}{R} n (n+1) \frac{\gamma - 1}{\gamma} C_p T_m \left(\frac{\Delta V}{V_m}\right)^2 \qquad (I.29)$$

The ratio of the orifice effect to the phase shift effect is found by dividing (I.27) by (I.21) to be equal to the polytropic constant n:

$$\frac{Q_{Lo}}{Q_{Lp}} = n \qquad (I.30)$$

APPENDIX II
PISTON RING FRICTION

Consider one of the two pumping piston rings (say the upper one) of a unidirectional set in a double acting rig and the variable volume above it. The ring is moving up and down with a substantially harmonic motion of stroke (S) so that its instantaneous position (x) is:

$$x = \frac{S}{2} \cos \omega t \qquad \text{(II.1)}$$

where ω is the angular speed and t is time.

This motion of the piston changes the volume (V) above the ring as follows:

$$V = V_m - \Delta V \cos \omega t \qquad \text{(II.2)}$$

where V_m is the mean volume and ΔV is the volume variation amplitude.

The gas is being compressed in a polytropic process with constant (n) so that its instantaneous pressure (p) is:

$$p = p_m + \Delta p \cos \omega t \qquad \text{(II.3)}$$

where p_m is the mean pressure and Δp is the pressure variation amplitude

The relation between the instantaneous volume (V) and the instantaneous pressure (p) for a polytropic process with constant (n) is:

$$pV^n = \text{const.} = p_m V_m^{\,n} \qquad \text{(II.4)}$$

Substitution of (2) and (3) in (4) yields:

$$p_m V_m^{\,n} \left(1 + \frac{\Delta p}{p_m} \cos \omega t\right) \left(1 - \frac{\Delta V}{V_m} \cos \omega t\right)^n = p_m V_m^{\,n}$$

or:

$$1 + \frac{\Delta p}{p_m} \cos \omega t = \left(1 - \frac{\Delta V}{V_m} \cos \omega t\right)^{-n} \qquad \text{(II.5)}$$

The right hand side may be expanded into a series with higher order terms in $(\frac{\Delta V}{V_m})$ neglected:

$$1 + \frac{\Delta p}{p_m} \cos \omega t = 1 + n \frac{\Delta V}{V_m} \cos \omega t + \text{H.O.T.}$$

This yields the following relation between the relative pressure and volume variation amplitudes:

$$\frac{\Delta p}{p_m} \approx n \frac{\Delta V}{V_m} \tag{II.6}$$

The pressure on the other side of the ring and in the groove is the maximum pressure of the variable volume: $p_m + \Delta p$.

The outward normal force (N) on the ring, forcing it at the wall is (as seen in Figure II-1):

$$N = \pi Dh[(p_m + \Delta p) - \tfrac{1}{2}\{(p_m + \Delta p) + (p_m + \Delta p \cos \omega t)\}] = \tfrac{1}{2}\pi Dh\Delta p\,(1 - \cos \omega t) \tag{II.7}$$

where D is the mean diameter of the piston ring and h is its axial thickness.

The friction force (F) is proportional to the normal force (N) with the friction coefficient (f) as the proportionality constant. F acts always in a direction opposite the piston speed ($\dot{x}$)

$$F = \tfrac{1}{2}\pi Dh\Delta pf\,(1 - \cos \omega t) \frac{|\sin \omega t|}{\sin \omega t} \tag{II.8}$$

The work (W) performed against the friction is:

$$dW = -F \frac{dx}{d\alpha} d\alpha = -\tfrac{1}{2}\pi Dh\Delta pf(1 - \cos\alpha) \frac{|\sin \alpha|}{\sin \alpha} (-\frac{S}{2} \sin\alpha)\, d\alpha =$$

$$= \tfrac{1}{4}\pi DhSf\Delta p(1 - \cos\alpha)\,|\sin \alpha|\, d\alpha \tag{II.9}$$

where $\alpha \equiv \omega t$

$$p = p_m + \Delta p \cos \omega t$$

$$\hat{p} = p_m + \Delta p$$

$$F_i = \pi Dh\hat{p} = \pi Dh\,(p_m + \Delta p)$$

$$F_o = \tfrac{1}{2}\ Dh(p + \hat{p}) = \pi\, Dh\,[p_m + \tfrac{1}{2}\Delta p\,(1 + \cos \omega t)]$$

$$N = F_i - F_o = \tfrac{1}{2}\pi Dh\Delta p\,(1 - \cos \omega t)$$

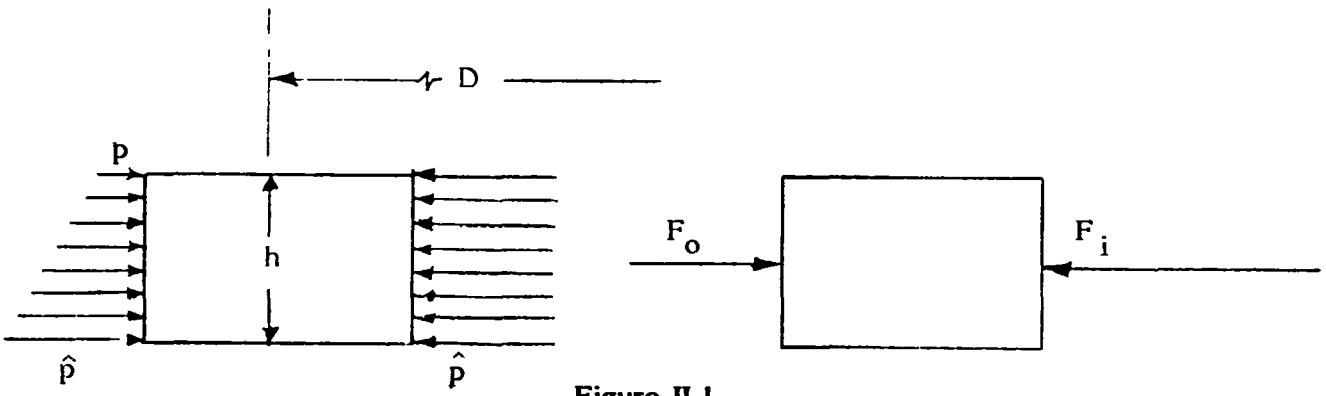

Figure II.1

Lateral Gas Forces on a Pumping Piston Ring

p = Instantaneous variable gas pressure

$\hat{p}$ = Maximum pressure

F_o = Pressure force acting on the OD of the ring

F_i = Pressure force acting on the ID of the ring

The work per cycle is achieved by integration of (9) over the entire cycle:

$$W = \int_0^{2\pi} \frac{dW}{d\alpha}\, d\alpha = 2 \int_0^{\pi} \frac{dW}{d\alpha}\, d\alpha = \pi\, DhSf\Delta p \qquad (II.10)$$

The same consideration applies to the other ring and hence the total piston ring friction loss (Q_f) in the rig is twice the amount of equation (10). Also, substitution of (6) yields:

$$Q_f = 2\pi\, DhSf p_m^{\,n} \left(\frac{\Delta V}{V_m}\right) \qquad (II.11)$$

APPENDIX III

Metallographic Inspection of Heat Pipe #2

Coulson M. Scheuermann
NASA Lewis Research Center
Cleveland, Ohio

Construction

This heat pipe contained no getter; therefore, no getter bucket or tube was included in its construction. The 27 1/2 inch (70 cm.) long tube body of the heat pipe was of type 321 stainless steel tube stock, 1 1/2 inch (3.8 cm.) diameter with a 0.049 inch (0.12 cm.) wall thickness.

Top and bottom caps were machined from type 304 stainless steel plate stock. The bottom cap was TIG-welded to the tube body. The top cap had a 1/4 inch (0.64 cm.) diameter type 304 stainless steel evacuation tube welded into it. This small tube had a valve attached to allow air addition.

The wick was a rolled tube of type 316 stainless steel, 0.002 inch (0.005 cm.) diameter wire, 165 mesh screen. The wick was inserted into the bottom of the tube body and held in place by a coiled 1/16 inch (0.16 cm.) diameter nichrome wire spring.

Sixteen grams of sodium were dropped into the pipe prior to closure. The top cap was then TIG-welded in place.

Operation

Heat pipe #2 (figures 4.1 and 4.2, also table 4.1) operated for a total 3,142 hours at 800°C. Starting at 2,158 hours of operation, a series of doses of air, about 2.0 Ncc each, were bled into the heat pipe. About 116 Ncc of total air volume was introduced. Full heat pipe operation recovered within 15 to 20 hours after each dose.

Metallographic Inspection

The heat pipe was cut into sections for visual inspection as shown in figure III-1. Specific areas were then chosen for chemical and metallographic analysis.

The dark deposit visible near the bottom of the heat pipe in figure III-1, and enlarged in figure III-2, was removed for chemical analysis.

Sections from the heat pipe were cut for metallographic inspection from the condenser and various locations down to the bottom end cap. These pieces were given a coating of copper, mounted in epoxy and examined using an electron microscope.

Results and Discussion

Chemical analysis of the dark deposit in figure III-2 revealed it to be primarily copper, with minor amount of iron, manganese, chronium and sodium. It is believed that this was caused by the inadvertent introduction of copper filings from tools used during the pipe construction.

Metallographic and electron microscopic examination of samples from the heat pipe condenser end did not reveal any serious structural problems. There was a slight surface effect extending to a depth of about 0.0009 inch (0.002 cm.), especially along grain boundaries (figure III-3). This effect was general along the entire heat pipe wall. It seemed related to a loss of Ni, and possibly, C from the wall.

More extensive attack by the sodium appeared in the evaporator section at the bottom of the pipe. The nichrome wire in this location suffered grain boundary attack and removal of Ni and C to about 0.002 inch (0.006 cm.) depth in the region where the wire contacted the wick, but none away from the wick. The wick itself was highly attacked (figure III-4). The bottom end cap experienced a greater degree of attack than did the pipe wall. Here the attack was to a depth of about 0.002 inch (0.006 cm.) depth.

Considering the intentional lack of control over cleanliness and sodium purity, the operation of this heat pipe demonstrated the ruggedness and tolerance of this system. Even though there were obvious plugged and corroded portions of the wick in the evaporator area, the pipe did not exhibit signs of operational distress. Corrosion, although present, did not hamper the operation, nor did it proceed to the extent where it could cause failure. Even intentional air leakage did not seriously hamper operation, since the pipe operation soon recovered to pre-leakage performance.

This pipe had many different materials in its construction. If all parts were made from a common, relatively corrosion resistant material, potential problems resulting from corrosion could be minimized.

Conclusions

The main conclusions to be reached from these test results are:

1. Corrosion did occur, but it was not severe enough to cause failure. It did not appear to be a serious problem for the pipe wall or spring;
2. Corrosion of the wick in the evaporator section could become an operational problem;
3. Potential corrosion problems could be reduced by using a single material of construction for all heat pipe parts;
4. Satisfactory heat pipe operation can be achieved without meticulous cleanliness or sodium purity control.

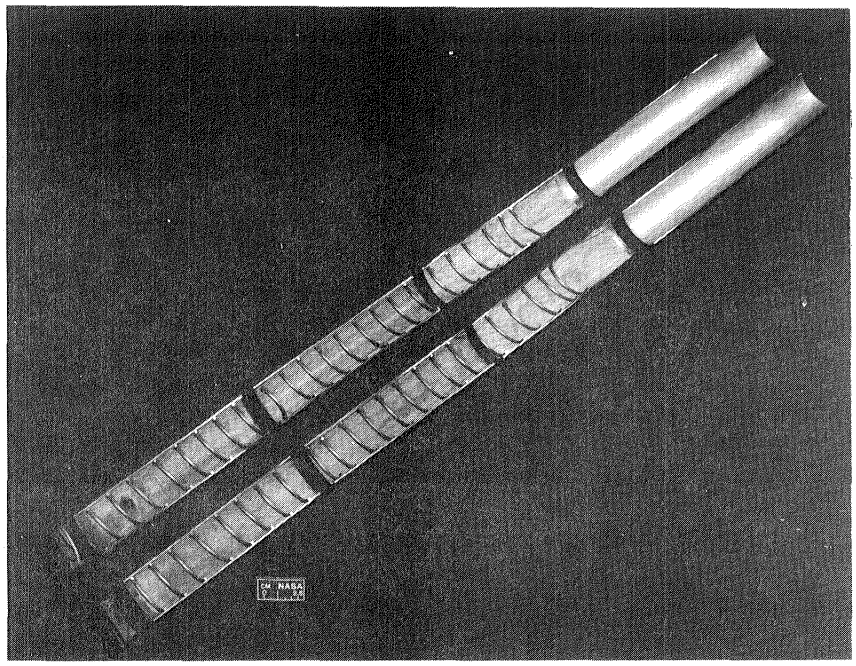

Figure III-1.

Overall view of sectional heat pipe #2.

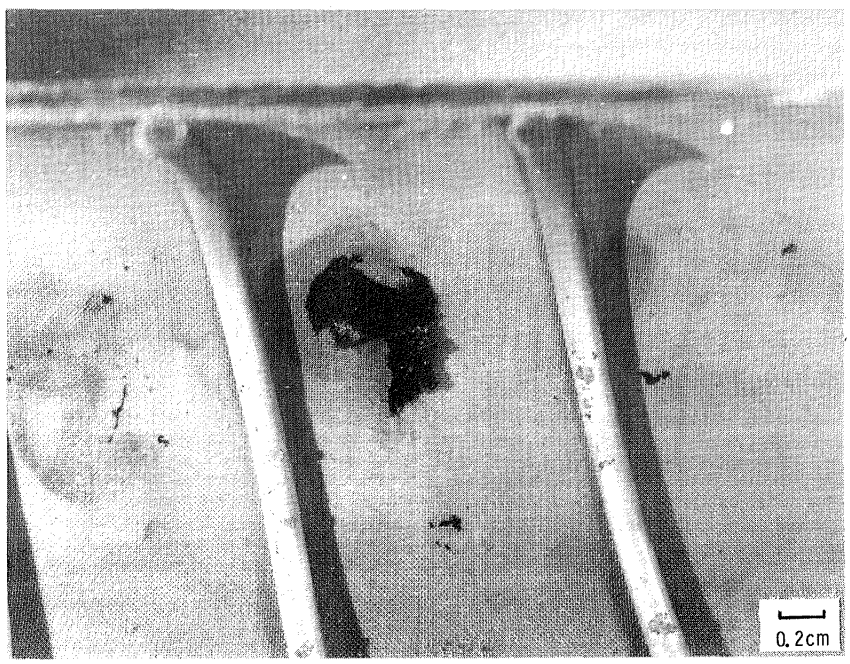

Figure III-2.

View of sectioned heat pipe #2
showing the dark deposit.

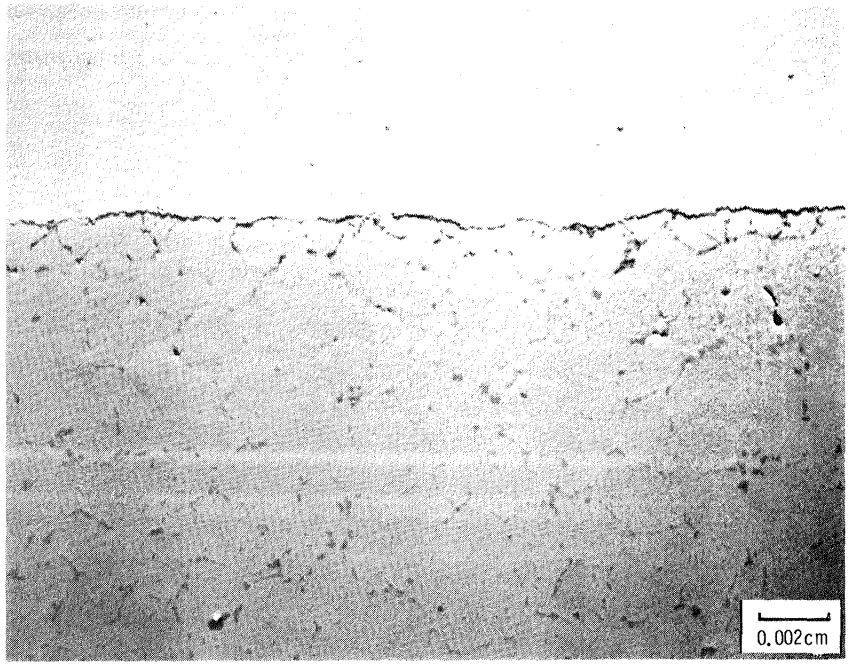

Figure III-3.

A typical electron photomicograph of the wall of heat pipe #2 in the condenser section showing the slight corrosion attack.

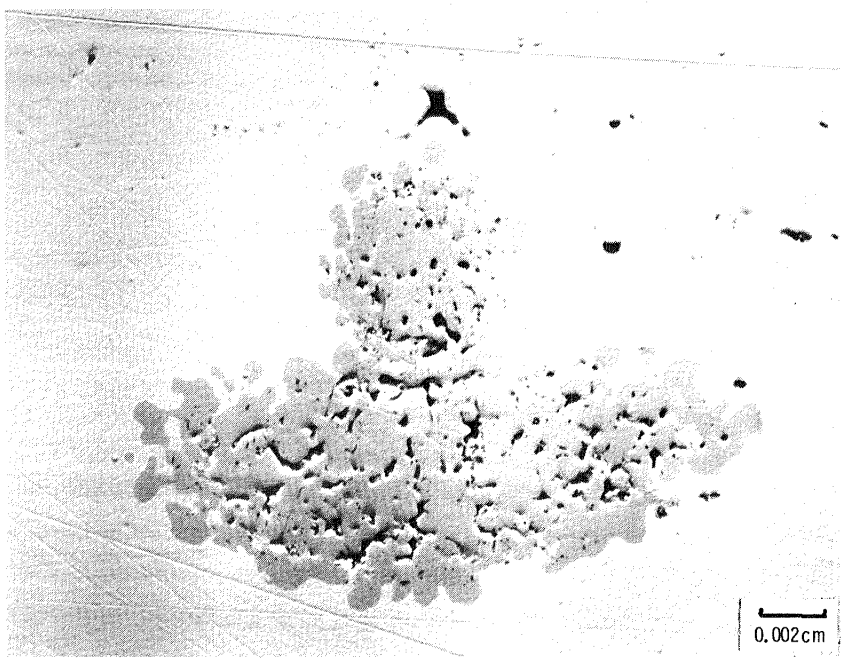

Figure III-4.

An electron photomicrograph of the corroded wick in the evaporator section of heat pipe #2.

1 Report No	2 Government Accession No	3 Recipient's Catalog No
NASA CR-174994		

4 Title and Subtitle	5 Report Date
Experimental Assessment of Advanced Stirling Component Concepts	October 1985
	6 Performing Organization Code
7 Author(s)	8 Performing Organization Report No
Benjamin Ziph	
	10 Work Unit No
9 Performing Organization Name and Address	11 Contract or Grant No
Stirling Thermal Motors, Inc. 2841 Boardwalk Ann Arbor, Michigan 48104	DEN 3-351
	13 Type of Report and Period Covered
12 Sponsoring Agency Name and Address	Contractor Report
U.S. Department of Energy Office of Vehicle and Engine R&D Washington, D.C. 20545	14 Sponsoring Agency Code Report No. DOE/NASA/0351-1

15 Supplementary Notes

Final Report. Prepared under Interagency Agreement DE-AI01-77CS51040. Project Manager, J. Cairelli, Power Technology Division, NASA Lewis Research Center, Cleveland, Ohio 44135.

16 Abstract

This final report presents the results of an experimental assessment of some advanced Stirling engine component concepts. Under this program, high performance piston rings, reciprocating oil scrapers and heat pipes with getters and with mechanical couplings were tested. The tests yielded the following results:

(1) Bonded, split, pumping piston rings, in preliminary testing, proved a promising concept, exhibiting low leakage and friction losses. Solid piston rings proved impractical in view of their sensitivity to the operating temperature.

(2) A babbit oil scraper in a compliant housing performed well in atmospheric endurance testing. In pressurized tests the scraper did not perform well as a containment seal. The latter tests suggest modifications which may adapt Ti successfully to that application.

(3) Heat pipe endurance tests indicated the adequacy of simple, inexpensive fabrication and filling procedures. Getters were proved to increase the tolerance of the heat pipes to the presence of air,and commercially available couplings were demonstrated to be suitable for heat pipe application.

In addition to the above tests, the program also included a design effort for a split shaft applicable to a swashplate driven engine with a pressurized crankcase. The design is aimed, and does accomplish, an increase in component life to more than 10 000 hr.

17 Key Words (Suggested by Author(s))	18 Distribution Statement
Stirling engines; Heat pipes; Piston rings; Scraper seals; Test data; Split shaft design; Swashplate	Unclassified - unlimited STAR Category 85 DOE Category UC-96

19 Security Classif (of this report)	20 Security Classif (of this page)	21 No of pages	22 Price*
Unclassified	Unclassified	105	A06

*For sale by the National Technical Information Service, Springfield, Virginia 22161

End of Document